LETTER Communicated by Klaus Pawelzik

Dynamics of the Firing Probability of Noisy Integrate-and-Fire Neurons

Nicolas Fourcaud
fourcaud@biomedicale.univ-paris5.fr
Nicolas Brunel
brunel@biomedicale.univ-paris5.fr
Laboratoire de Physique Statistique, École Normale Supérieure, 75231 Paris Cedex 05, France, and Neurophysique et Physiologie du Système Moteur, UFR biomédicale, Université Paris 5 René Descartes 45, 75006 Paris, France

Cortical neurons in vivo undergo a continuous bombardment due to synaptic activity, which acts as a major source of noise. Here, we investigate the effects of the noise filtering by synapses with various levels of realism on integrate-and-fire neuron dynamics. The noise input is modeled by white (for instantaneous synapses) or colored (for synapses with a finite relaxation time) noise. Analytical results for the modulation of firing probability in response to an oscillatory input current are obtained by expanding a Fokker-Planck equation for small parameters of the problem—when both the amplitude of the modulation is small compared to the background firing rate and the synaptic time constant is small compared to the membrane time constant. We report here the detailed calculations showing that if a synaptic decay time constant is included in the synaptic current model, the firing-rate modulation of the neuron due to an oscillatory input remains finite in the high-frequency limit with no phase lag. In addition, we characterize the low-frequency behavior and the behavior of the high-frequency limit for intermediate decay times. We also characterize the effects of introducing a rise time to the synaptic currents and the presence of several synaptic receptors with different kinetics. In both cases, we determine, using numerical simulations, an effective decay time constant that describes the neuronal response completely.

1 Introduction

Noise has an important impact on the dynamics of the discharge of neurons in vivo. Neurons in the cerebral cortex recorded in vivo show very irregular firing in a large range of firing rates (Softky & Koch, 1993), and there is a wide variability in the spike trains of neurons from trial to trial. There is evidence that a large part of the noise experienced by a cortical neuron is due to the intensive and random bombardment of synaptic sites. Neurons in cortical networks in vivo in awake animals (Burns & Webb, 1976) and anesthetized

animals (Destexhe & Paré, 1999) are spontaneously active and emit spikes at rates of about 5–10 Hz in an approximately Poissonian way. Due to the large number of synaptic contacts (around 10,000), a cortical neuron thus receives a huge bombardment of spikes in an interval corresponding to its integration time constant (about 20 ms; see McCormick, Connors, Lighthall, & Prince, 1985).

The impact of noise on neuronal dynamics can be studied in detail in a simple spiking neuron model, the integrate-and-fire (IF) neuron (Lapicque, 1907; Knight, 1972; Tuckwell, 1988). Knight (1972) pioneered the study of the effect of noise on the dynamics of such a spiking neuron. The noise model he studied was a simplified model in which the threshold is drawn randomly after each spike. Gerstner (2000) extended these results and studied both slow noise models, in which either the threshold or the reset is drawn randomly after each spike, and fast escape rate noise models. Phase noise has also been used to study synchrony in networks of coupled oscillators (Abbott & van Vreeswijk, 1993). However, none of these noise models can represent in a realistic way synaptic noise as experienced by cortical neurons. Synaptic currents provoked by a single spike recorded in slice experiments have a fast rise time (often less than 1 ms) and a slower decay time (in the range of 2 to 100 ms depending on the type of receptor; Destexhe, Mainen, & Sejnowski, 1998). Common synaptic currents are excitatory glutamatergic currents, which can be mediated by either fast AMPA receptors (decay of order 2 ms) or slower NMDA receptors (decay of order 50–100 ms) and inhibitory GABAergic currents, whose fast component is mediated by the $GABA_A$ receptor (decay of order 5–10 ms). Such synaptic currents can be described by a simple system of ordinary differential equations (Destexhe et al., 1998; Wang, 1999).

In this article, we study the impact of noise originating from realistic synaptic models on the dynamics of the firing probability of a spiking neuron. We explore three levels of complexity for the synaptic currents: (1) instantaneous (delta function) synaptic current, (2) synaptic current with an instantaneous jump followed by an exponential decay with time constant τ_s, and (3) synaptic current described by a difference of exponentials, with a rise time τ_r and decay time τ_s.

The dynamics of the firing probability of a neuron receiving a bombardment of spikes through such synaptic currents is studied in the framework of the diffusion approximation (see in the neuronal context Tuckwell, 1988; Amit & Tsodyks, 1991). This approximation is justified when a large number of spikes arrive through synapses that are weak compared to the magnitude of the firing threshold, which is the relevant situation in cortex. In the diffusion approximation, the random component in the synaptic currents can be treated as white noise in the case of instantaneous synapses. On the other hand, when synapses have a finite temporal width, as in the more realistic models, synaptic noise has a finite correlation time and thus becomes "colored" noise. Thanks to the diffusion approximation, the dynamics of

firing probability can be studied in the framework of the Fokker-Planck theory (Risken, 1984). The dynamics at the network level has been studied analytically recently in the white noise case by Brunel and Hakim (1999) and Brunel (2000). Similar population density approaches have been investigated by Knight, Omurtag, and Sirovich (2000), Nykamp and Tranchina (2000, 2001), and Haskell, Nykamp, and Tranchina (2001).

Using the tools of the dynamical linear response theory (Knight, 1972; Gerstner, 2000; Brunel, Chance, Fourcaud, & Abbott, 2001), we study the dynamics of the firing discharge in response to a synaptic current composed of the sum of a stationary stochastic background current, which by itself provokes a background firing rate ν_0, and of a small oscillatory component at frequency ω. The knowledge of the response at all frequencies allows us to determine the response of the neuron to arbitrary stimuli, in the linear approximation. Knight (1972) had shown that integrate-and-fire (IF) neurons have a finite response even in the high-frequency limit for the simplified noise model investigated. Surprisingly, recent studies have shown that in the case of white noise, the amplitude of the firing-rate modulation at high frequencies decays as $1/\sqrt{\omega}$, with a phase lag that approaches 45 degrees in that limit (Brunel & Hakim, 1999; Brunel et al., 2001); when a more realistic synaptic noise is taken into account, the amplitude of the firing-rate modulation is finite even in the high-frequency limit, and the phase lag is eliminated (Brunel et al., 2001).

In this article, we study in more detail how the characteristics of the synaptic currents affect the neuronal response. We start with a detailed report of the calculations leading to the results in the colored noise case. This is done with two types of IF neurons: with or without leak. Using analytical calculations and numerical simulations, we then proceed to study how the high-frequency limit depends on the synaptic decay time, the effect of the synaptic rise time, and the effects of synaptic currents mediated by different receptors with different kinetics, as is the case in neurons in the cerebral cortex.

Section 2 describes the models we use. In the following sections, we present the analytical calculations leading to the linear dynamical response of the two types of IF neurons. In section 4, analytical methods are presented, and the stationary firing probability is calculated. Then, in section 5, we calculate analytically the linear dynamical responses in the low- and high-frequency limits. Numerical simulations are used to obtain the response in the full-frequency range and in the more complicated synaptic filtering cases. Finally, we discuss our results in section 6.

2 Models

2.1 The Integrate-and-Fire Model Neurons. The IF model was introduced long ago by Lapicque (1907). Due to its simplicity, it has become one of the canonical spiking renewal models, since it represents one of the

few neuronal models for which analytical calculations can be performed. It describes basic subthreshold electrical properties of the neuron. It is completely characterized by its membrane potential below threshold. Details of the generation of an action potential above the threshold are ignored. Synaptic and external inputs are summed until it reaches a threshold where a spike is emitted. The general form of the dynamics of the membrane potential $V(t)$ in IF models can be written as

$$C\frac{dV}{dt} = I_l(V) + I_s(V,t) + I_e(t), \tag{2.1}$$

where I_s is the synaptic current, I_e is an external current directly injected in the neuron, I_l is a leak current, and C is the membrane capacitance. In the following, I_s will represent the noisy inputs due to background synaptic activity, and I_e will represent an oscillatory input. In vivo, oscillatory inputs arrive through synapses and should therefore be incorporated into I_s. However, for the purpose of the calculations detailed here, it is convenient to extract the oscillatory component from the noise and inject it directly to the cell. We will then come back in the discussion to the neuronal response to oscillatory inputs filtered through synapses.

When the membrane potential reaches a fixed threshold θ, the neuron emits a spike and is reset to V_r. We could also introduce an absolute refractory period (ARP) after the emission of a spike during which the neuron is silent and does not sum the input signal. For simplicity, we set the ARP to zero in the following. In the most interesting region of firing rates far from saturation, the inclusion of ARP will affect the results only mildly.

Several variants of this model have been considered in the literature. The simplest integrate-and-fire neuron (SIF) has no leak current: $I_l(V) = 0$. Thus, in the absence of inputs, the neuron stays indefinitely at its initial value. The leaky, or forgetful, integrate-and-fire neuron (LIF) has a leak current $I_l(V) = -g(V - V_L)$, where g is the leak conductance and V_L the resting potential. We note $C/g = \tau_m$ where τ_m is the membrane time constant. In all calculations, we set $V_L = 0$. In simulations, we use $V_L = -70$ mV.

Dividing both sides by g, we can reexpress equation 2.1 as

$$\tau_m\frac{dV}{dt} = f(V) + I_s(V,t) + I_e(t), \tag{2.2}$$

where $f(V) = 0$ for the SIF, $f(V) = -V$ for the LIF, and g has been absorbed in the currents I_s and I_e, which are now expressed in units of voltage. Note that in the SIF, τ_m is an arbitrary parameter, used only to unify the description with the LIF. Thus, results for the SIF will be completely independent of that parameter.

2.2 Models of Synaptic Filtering. Many mathematical descriptions of synaptic currents have been proposed, from overly simple to very realistic

(for a review, see Destexhe et al., 1998). Realistic models of the synaptic current $I_s(V,t)$ depend on the membrane potential V through $I_s(V,t) = g(V - V_{rev})s(t)$, where g is the synaptic conductance, V_{rev} is the reversal potential of the synapse, and $s(t)$ describes the temporal dynamics of the synapse. In the following, we ignore the driving force $V - V_{rev}$ for simplicity and consider current rather than conductance changes at synaptic sites. Thus, synaptic currents become independent on voltage.

The synaptic models we consider follow.

2.2.1 Instantaneous (Delta Function) Synapses. If we neglect the synaptic time constants compared to the neuronal time constants, postsynaptic currents (PSCs) can be described by delta functions, and the synaptic input $I_s(t)$ can be described by

$$I_s(t) = \sum_{i=1}^{N_s} J_i \sum_k \delta(t - t_i^k)\tau_m. \tag{2.3}$$

The sum over i corresponds to a sum over all synapses, N_s is the number of synaptic connections (typically 10, 000), J_i is the efficacy of synapse i in mV (amplitude of the postsynaptic potential), the sum over k corresponds to a sum over presynaptic spikes of each synapse, and t_i^k is the time where the kth presynaptic spike arrives at the synapse i.

2.2.2 Synapses with Instantaneous Jump and Exponential Decay. In reality, postsynaptic currents have a finite width that can be of the same order of magnitude or even larger than the membrane time constant. A more accurate representation of synaptic inputs consists of an instantaneous jump followed by an exponential decay with a time constant τ_s. This can be described by the following equation:

$$\tau_s \frac{dI_s}{dt} = -I_s(t) + \sum_{i=1}^{N_s} J_i \sum_k \delta(t - t_i^k)\tau_m. \tag{2.4}$$

In such a description, the rise time of the synaptic current is neglected. This is justified by the observation that the rise time of a synapse is typically very short compared to the relaxation time. Moreover, such a description implicitly assumes τ_s to be the same for all synapses.

2.2.3 Synaptic Currents with Different Decay Time Constants. Synaptic inputs to a cortical neuron come from different types of receptors with different temporal characteristics. Common types of receptors are AMPA, NMDA, and GABA receptors. AMPA receptors have synaptic time constants of the order of 2 ms (Hestrin, Sah, & Nicoll, 1990; Sah, Hestrin, &

Nicoll, 1990; Spruston, Jonas, & Sakmann, 1995; Angulo, Rossier, & Audinat, 1999). $GABA_A$ receptors have longer time constants (typically 5–10 ms; Salin & Prince, 1996; Xiang, Huguenard, & Prince, 1998; Gupta, Wang, & Markram, 2000). Finally, NMDA currents are the slowest, with decay time constants of about 100 ms (Hestrin et al., 1990; Sah et al., 1990). Thus, it is of interest to consider synaptic inputs that are combinations of inputs coming through different receptors.

Such synaptic inputs can be described by a system of equations,

$$I_s(t) = I_{s_1}(t) + I_{s_2}(t) \tag{2.5}$$

$$\tau_{s_1} \frac{dI_{s_1}}{dt} = -I_{s_1}(t) + \sum_{i=1}^{N_{s_1}} J_{1_i} \sum_k \delta(t - t_{1_i}^k)\tau_m \tag{2.6}$$

$$\tau_{s_2} \frac{dI_{s_2}}{dt} = -I_{s_2}(t) + \sum_{i=1}^{N_{s_2}} J_{2_i} \sum_k \delta(t - t_{2_i}^k)\tau_m, \tag{2.7}$$

where s_i, $i = 1, 2 \ldots$, represent different types of synaptic receptors. In particular we will consider the situation in which two types of receptors are present: AMPA and GABA.

2.2.4 Synapses with Rise and Decay Times. Finally, the effects of a finite rise time can be included by a third variable in the system of equations describing neuronal dynamics. A simple way to introduce a rise time is to consider this system of equations:

$$\tau_s \frac{dI_s}{dt} = -I_s(t) + I_r(t) \tag{2.8}$$

$$\tau_r \frac{dI_r}{dt} = -I_r(t) + \sum_{i=1}^{N_s} J_i \sum_k \delta(t - t_i^k)\tau_m. \tag{2.9}$$

Figure 1 shows different postsynaptic currents (PSCs) with different rise times. Note that our description of the current with a rise time is similar to other kinetic descriptions (see Destexhe et al., 1998 or Wang, 1999), except that we do not take into account the saturation of I_s. Neglecting saturation is justified when presynaptic firing rates are low, which is the prevalent situation during spontaneous activity in the cortex.

3 Analytical Methods

3.1 Diffusion Approximation. Neurons usually have synaptic connections from tens of thousands of other neurons. Thus, even when neurons fire at low rates, a neuron receives a large amount of spikes in an interval corresponding to its integration time constant. If we assume these inputs

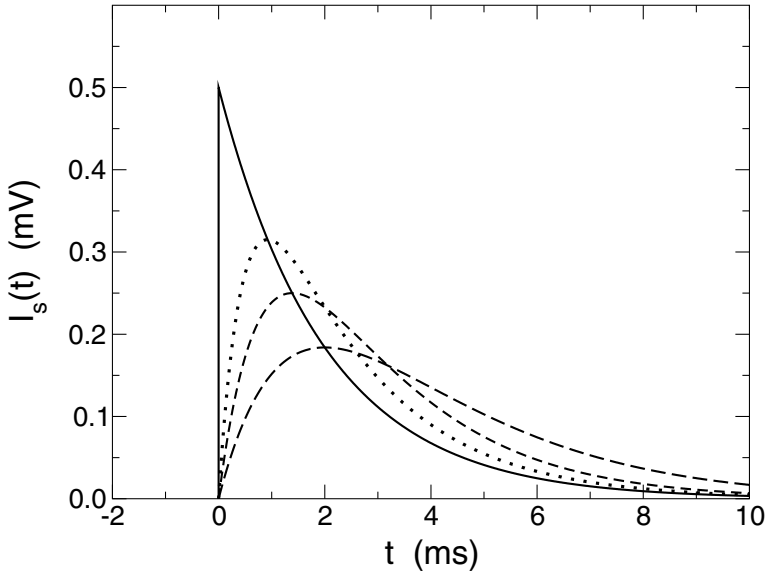

Figure 1: Single PSCs for synapses with $\tau_s = 2$ ms and different rise time constants $\tau_r = 0$ ms (solid line), $\tau_r = 0.5$ ms (dotted line), $\tau_r = 1$ ms (dashed line), $\tau_r = 2$ ms (long-dashed line).

are Poissonian and uncorrelated and the amplitude of the depolarization due to each input is small—$\langle J_i \rangle \ll \theta - V_r$, where $\langle . \rangle$ is the average over the input synapses—we can use the diffusion approximation. It consists in approximating fluctuations around the mean of the total input spike train by a gaussian white noise,

$$\sum_{i=1}^{N_s} J_i \sum_k \delta(t - t_i^k) \approx \tilde{\mu} + \tilde{\sigma}\eta(t) \tag{3.1}$$

where $\tilde{\mu}$ is proportional to the mean of the synaptic input and η is a gaussian random variable satisfying $\langle \eta(t) \rangle = 0$ and $\langle \eta(t)\eta(t') \rangle = \delta(t - t')$. $\tilde{\sigma}$ characterizes the amplitude of the noise.

If we assume the mean activation rate for each synapse is ν, we have

$$\tilde{\mu} = \langle J_i \rangle N_s \nu, \quad \tilde{\sigma}^2 = \langle J_i^2 \rangle N_s \nu. \tag{3.2}$$

Note that $\tilde{\mu}$ is in units of mV.ms^{-1} and $\tilde{\sigma}$ in mV.ms$^{-\frac{1}{2}}$.

Consequently, when synapses are instantaneous (relaxation synaptic time equals zero), the noise in the current is equivalent to white noise, but when the synaptic current has a temporal width, the noise is equivalent to colored

noise. Using the diffusion approximation, the neuronal dynamics is fully described by the following systems of stochastic equations:

Instantaneous Synapses:

$$\tau_m \frac{dV}{dt} = f(V) + \mu + \sigma\sqrt{\tau_m}\eta(t) + I_e(t) \tag{3.3}$$

in which μ and σ are:

$$\mu = \tilde{\mu}\tau_m = \langle J_i \rangle N_s \nu \tau_m, \quad \text{and} \quad \sigma^2 = \tilde{\sigma}^2 \tau_m = \langle J_i^2 \rangle N_s \nu \tau_m \tag{3.4}$$

and are both in mV.

Exponentially decaying synapses:

$$\tau_m \frac{dV}{dt} = f(V) + I_s(t) + I_e(t) \tag{3.5}$$

$$\tau_s \frac{dI_s}{dt} = -I_s(t) + \mu + \sigma\sqrt{\tau_m}\eta(t). \tag{3.6}$$

3.2 Neuronal Frequency Response. The main goal of this article is to determine the neuronal response to an oscillatory input in presence of a realistic synaptic noise. Figure 2 shows an example of numerical simulations of 2000 neurons receiving a common oscillatory current input but with noise inputs that are uncorrelated from neuron to neuron (upper panel). We see on the raster (middle panel) that the neurons do not emit spikes regularly at the input frequency but discharge quite randomly. Actually, it is the instantaneous firing rate (the firing probability) of each neuron that oscillates in time (bottom panel). In the following, we compute the amplitude of the oscillatory response and its phase shift.

The instantaneous firing rate $\nu(t)$ of the neuron is computed in two steps. We start with a stationary input $I_e(t) = 0$. The resulting firing probability is $\nu(t) = \nu$ (see section 4). Then we introduce a small oscillatory input $I_e(t) = \epsilon\mu e^{i\omega t}$, $\epsilon \ll 1$, and we compute the linear (first-order) correction to the instantaneous firing rate $\nu(t) = \nu[1 + \epsilon\hat{n}(\omega)e^{i\omega t}]$ (see section 5). In both cases, we first make calculations for instantaneous currents ($\tau_s = 0$). Then we compute the first-order correction due to the introduction of the synaptic decay time ($\tau_s > 0$).

In each section, we will present in the main text only the main steps and the results. Details of the calculations can be found in the appendixes.

3.3 Fokker-Planck Equation and Its Boundary Conditions. The analytical methods we use consist of solving the dynamical Fokker-Planck equation associated with the stochastic equations given in section 3.1. We look

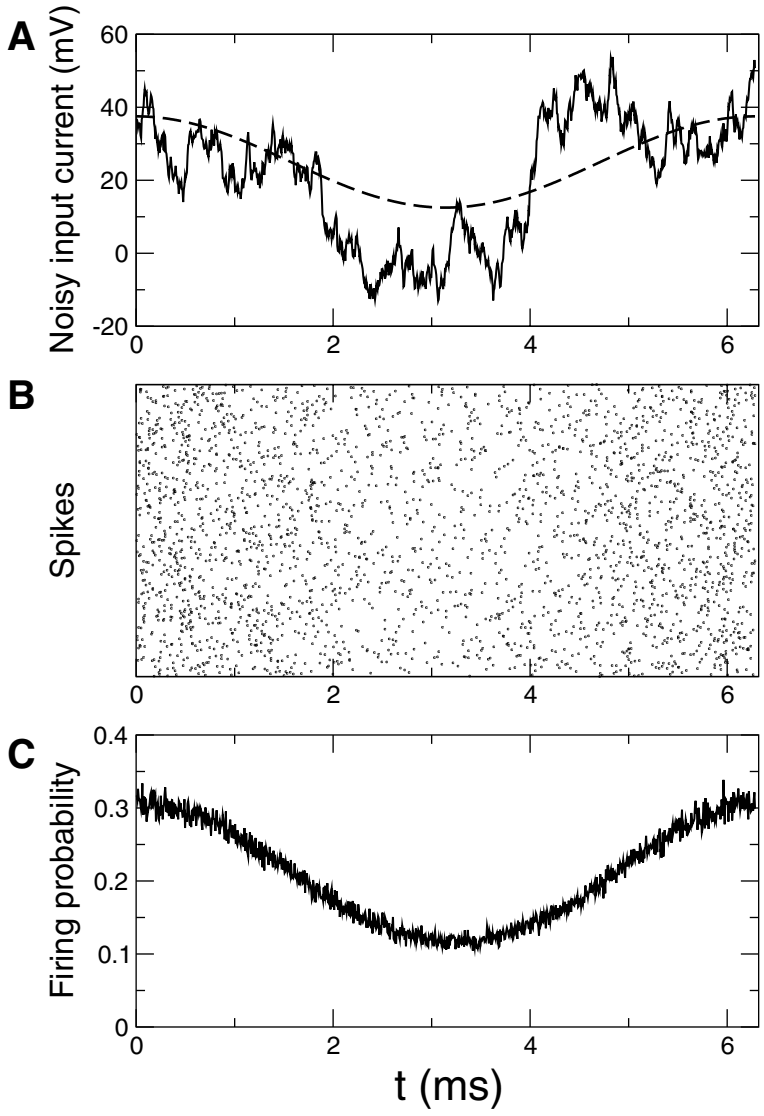

Figure 2: Firing probability response to oscillatory current with noise. (A) Oscillatory current, I_e (dashed line), and noisy oscillatory current, $I_e + I_s$ (solid line). (B) Raster of 2000 neurons subject to oscillatory current with uncorrelated noise. (C) Firing probability of the neuron calculated in bins of 6 μs.

for the probability density $\mathcal{P}(V, I_s, t)$ of voltage V and synaptic current I_s at time t. We note

$$\mathcal{P}(V, I_s, t) = P(V, I_s) + \epsilon \hat{P}(V, I_s, \omega) e^{i\omega t} + O(\epsilon^2),$$

where P is the stationary part of $\mathcal{P}$ and $\hat{P}$ describes the part of $\mathcal{P}$ that oscillates at the same frequency as the current input. Since we will consider the limit of small perturbations around the stationary probability density function $\epsilon \ll 1$, we do not take into account higher-order terms in the expansion of $\mathcal{P}$, which would contain higher harmonics.

The dynamical Fokker-Planck equation can be written

$$\frac{\partial \mathcal{P}}{\partial t} + \frac{\partial J_V}{\partial V} + \frac{\partial J_{I_s}}{\partial I_s} = 0, \tag{3.7}$$

where J_V is the probability flux of $\mathcal{P}$ through V at fixed I_s and J_{I_s} is the probability flux of $\mathcal{P}$ through I_s at fixed V. The instantaneous firing rate is given by the sum of the probability flux through the firing threshold $V = \theta$ over I_s:

$$\nu(t) = \int J_V(\theta, I_s, t) dI_s. \tag{3.8}$$

In the case of instantaneous synapses ($\tau_s = 0$), $\mathcal{P}$ depends on V only, and the instantaneous firing rate simplifies to

$$\nu(t) = J_V(\theta, t). \tag{3.9}$$

When we introduce the synaptic relaxation time ($\tau_s > 0$), we face a more complex problem of solving a two-dimensional Fokker-Planck equation with a boundary limit on a semi-infinite line, as we will see in sections 4.1.3 through 4.2.3. The equation can be solved recursively using an expansion in $\sqrt{\tau_s/\tau_m}$, using analytical methods developed by Hagan, Doering, and Levermore (1989).

4 Stationary Firing Probability

We describe in this section the calculation of the firing rate and the probability density function (p.d.f.) of the neuronal membrane potential when it receives a stationary input: $I_e(t) = 0$. Note that the membrane potential of the leaky IF neuron with white noise is described by an Ornstein-Uhlenbeck process whose mean first passage time to threshold is well known (Tuckwell, 1988; Amit & Tsodyks, 1991). The solution for the simplest IF neuron with reflecting boundary condition at reset has been calculated by Fusi and Mattia (1999).

The calculation of the LIF stationary firing rate and of the p.d.f. when noise is white is given in Brunel and Hakim (1999). The calculation of the stationary firing rate when noise is colored has been performed in Brunel and Sergi (1998), assuming that the probability density of synaptic currents after the end of an absolute refractory period is gaussian. Here, we calculate the stationary firing rate with colored noise relaxing the assumption that Brunel and Sergi (1998) made. This gives a slight difference in the final formula for the firing probability.

In the case of the SIF neuron, we can show that the mean firing rate does not depend on the synaptic time constants (τ_r and τ_s) and depends only on the mean synaptic input. This result is given in appendix A. Here, we calculate the p.d.f. without and with relaxation time of the synapses. Indeed, we will see that to determine the dynamic properties of the neuron, we will need to know the first-order correction in τ_s of the stationary p.d.f.

4.1 White Noise. In this section, we calculate the p.d.f. of the IF neuron membrane potential without relaxation time of the synapses.

The stochastic equation, 3.3, is equivalent to the Fokker-Planck (FP) equation for the p.d.f. of the membrane potential, $P_0(V)$,

$$\tau_m \frac{\partial P_0}{\partial t} = \frac{\sigma^2}{2} \frac{\partial^2 P_0}{\partial V^2} - \frac{\partial}{\partial V}[(\mu + f(V))P_0], \tag{4.1}$$

where $f(V) = 0$ for the SIF neuron and $f(V) = -V$ for the LIF neuron.

The probability flux through V at time t is

$$J_V = \frac{\mu + f(V)}{\tau_m} P_0 - \frac{\sigma^2}{2\tau_m} \frac{dP_0}{dV}.$$

Since a spike is emitted each time V reaches θ and the neuron is then immediately reset to V_r, the boundary conditions for J_V are

$$J_V(\theta) = \nu_0 \tag{4.2}$$

$$J_V(V_{r+}) - J_V(V_{r-}) = \nu_0, \tag{4.3}$$

where ν_0 is the stationary instantaneous firing rate.

Equation 4.2, together with $P(V > \theta) = 0$, imply

$$P_0(\theta) = 0 \tag{4.4}$$

$$\frac{\partial P_0}{\partial V}(\theta) = -\frac{2\nu_0\tau_m}{\sigma^2} \tag{4.5}$$

$$P_0(V_{r+}) - P_0(V_{r-}) = 0 \tag{4.6}$$

$$\frac{\partial P_0}{\partial V}(V_{r+}) - \frac{\partial P_0}{\partial V}(V_{r-}) = -\frac{2\nu_0\tau_m}{\sigma^2}. \tag{4.7}$$

For the SIF neuron, the results are (see Abbott & van Vreeswijk, 1993, and appendix A.2 for details)

$$P_0(V) = \frac{\nu_0}{\tilde{\mu}}[1 - e^{\frac{2\tilde{\mu}(V-\theta)}{\tilde{\sigma}^2}} - \Theta(V_r - V)(1 - e^{\frac{2\tilde{\mu}(V-V_r)}{\tilde{\sigma}^2}})], \tag{4.8}$$

where Θ is the Heaviside function, $\Theta(x) = 1$ for $x > 0$ and 0 otherwise, and

$$\nu_0 = \frac{\tilde{\mu}}{\theta - V_r}. \tag{4.9}$$

The firing rate of the SIF neuron is independent on the magnitude of the noise $\tilde{\sigma}$.

For the LIF neuron, we have (Brunel & Hakim, 1999)

$$P_0(V) = \frac{2\nu_0\tau_m}{\sigma} \exp\left(-\frac{(V-\mu)^2}{\sigma^2}\right) \times \begin{cases} \int_{(V_r-\mu)/\sigma}^{(\theta-\mu)/\sigma} \exp(s^2)\, ds & \text{if } V < V_r \\ \int_{(V-\mu)/\sigma}^{(\theta-\mu)/\sigma} \exp(s^2)\, ds & \text{if } V > V_r, \end{cases} \tag{4.10}$$

in which the stationary firing rate ν_0 is obtained through the normalization condition,

$$\frac{1}{\nu_0} = \tau_m\sqrt{\pi} \int_{\frac{V_r-\mu}{\sigma}}^{\frac{\theta-\mu}{\sigma}} e^{s^2}(1 + \mathrm{erf}(s))\, ds \tag{4.11}$$

where erf is the error function (Abramowitz & Stegun, 1970).

4.2 Synaptic Noise.

4.2.1 Fokker-Planck Equation and Boundary Conditions. We consider now the system of equations 3.5 and 3.6. The Fokker-Planck equation becomes

$$\frac{\partial P}{\partial t} = \frac{1}{\tau_s}\left[\frac{\sigma^2\tau_m}{2\tau_s}\frac{\partial^2 P}{\partial I_s^2} + \frac{\partial}{\partial I_s}(I_s - \mu)P\right] - \frac{1}{\tau_m}\frac{\partial}{\partial V}[(I_s + f(V))P]. \tag{4.12}$$

The probability fluxes are

$$J_V = \frac{I_s + f(V)}{\tau_m}P \tag{4.13}$$

$$J_{I_s} = -\left(\frac{I_s - \mu}{\tau_s}\right)P + \frac{\sigma^2\tau_m}{2\tau_s^2}\frac{\partial P}{\partial I_s}. \tag{4.14}$$

The boundary conditions are now

$$J_V(\theta, I_s) = \nu(I_s) \tag{4.15}$$

$$J_V(V_{r+}, I_s) - J_V(V_{r-}, I_s) = \nu(I_s), \tag{4.16}$$

where $\nu(I_s)$ is the instantaneous firing rate of the neuron at current I_s. The total firing rate of the neuron is

$$\nu = \int_{-\infty}^{+\infty} \nu(I_s)\, dI_s. \tag{4.17}$$

Equation 4.13 and the fact that the probability flux must be nonnegative at $V = \theta$ for every I_s (no neuron comes back from above threshold) imply that $P(\theta, I_s) = 0$ for any $I_s + f(\theta) < 0$, which in turn implies

$$\nu(I_s) = 0, \quad \text{for all} \quad I_s + f(\theta) < 0. \tag{4.18}$$

On the other hand, $P(\theta, I_s)$ must be positive for $I_s + f(\theta) > 0$ for firing to occur. The boundary conditions on P can be written

$$(I_s + f(\theta))P(\theta, I_s) = \nu(I_s)\tau_m \tag{4.19}$$

$$(I_s + f(\theta))[P(V_{r+}, I_s) - P(V_{r-}, I_s)] = \nu(I_s)\tau_m. \tag{4.20}$$

We also need to specify boundary conditions on the I_s variable. Since the neuron can escape the phase plane only through $V = \theta$, the flux through I_s is going to 0 for large $|I_s|$. Thus, the boundary conditions on I_s are

$$\lim_{I_s \to \pm\infty} J_{I_s}(V, I_s) = 0, \tag{4.21}$$

which implies

$$\lim_{I_s \to \pm\infty} \frac{\partial P}{\partial I_s} = 0 \tag{4.22}$$

$$\lim_{I_s \to \pm\infty} I_s P = 0. \tag{4.23}$$

4.2.2 The Small τ_s Limit: Strategy. The two-dimensional Fokker-Planck equation, 4.12, can be solved using singular perturbation techniques in the small τ_s limit (Hagan et al., 1989). In that limit, the variance of I_s becomes proportional to $\sigma\sqrt{\frac{\tau_m}{\tau_s}}$. Thus, we define

$$k = \sqrt{\frac{\tau_s}{\tau_m}}, \tag{4.24}$$

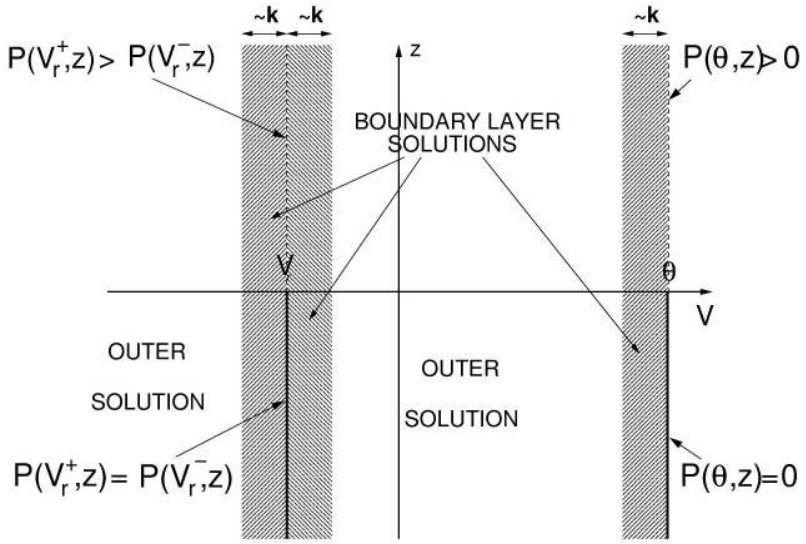

Figure 3: Sketch of the (V, z) plane with the boundary conditions and the areas where different solutions are computed: the outer solution far from the boundaries and the boundary layer solutions in areas of width k around the boundaries that satisfy the boundary conditions and match the outer solution outside the gray areas.

which will be used as a small parameter in which we will expand the FP equation, 4.12. We also define a new variable z:

$$I_s = \frac{\sigma z}{k} - f(\theta). \tag{4.25}$$

The advantage of this new variable is that it keeps a finite variance in the small τ_s limit.

The problem is complicated by the boundary conditions on the semi-infinite lines ($z < 0$) at $V = \theta$ and $V = V_r$ (see equation 4.18). The method consists of two steps. First, we look for a solution of the equation far from the boundaries: the outer solution. The outer solution is sufficiently far from the boundaries not to be affected by them. Second, we concentrate on narrow regions of width k around the boundaries (the boundary layers). We determine boundary layer solutions that satisfy the boundary conditions and reach exponentially the outer solution far from the boundaries. Figure 3 shows in the plane (V, z) the regions in which the different solutions will be calculated.

4.2.3 The p.d.f. of the SIF Neuron. The p.d.f. up to first order in k is (see section A.3 for details)

$$P(V,z) = \left(Q_0(V) + \sqrt{\frac{\tau_s}{\tau_e}} Q_1(V,z)\right) \frac{e^{-z^2}}{\sqrt{\pi}}, \tag{4.26}$$

with

$$Q_0(V) = \frac{\nu_0}{\tilde{\mu}}[1 - e^{\frac{2\tilde{\mu}(V-\theta)}{\tilde{\sigma}^2}} - \Theta(V_r - V)(1 - e^{\frac{2\tilde{\mu}(V-V_r)}{\sigma^2}})], \tag{4.27}$$

and

$$\tau_e = \frac{\tilde{\sigma}^2}{\tilde{\mu}^2} \tag{4.28}$$

represents the effective time constant of the SIF neuron.

Far from V_r and θ,

$$Q_1(V,z) = \frac{\nu_0}{\tilde{\mu}}[\alpha e^{\frac{2\tilde{\mu}(V-\theta)}{\tilde{\sigma}^2}} + 2z - \Theta(V_r - V)(\alpha e^{\frac{2\tilde{\mu}(V-V_r)}{\tilde{\sigma}^2}} + 2z)]. \tag{4.29}$$

When the membrane potential is close to the reset, ($V = V_r + O(k)$), or to threshold ($V = \theta + O(k)$), we have, using the reduced variables,

$$v = \frac{(V_r - V)}{\tilde{\sigma}\sqrt{\tau_s}}, \quad x = \frac{(\theta - V)}{\tilde{\sigma}\sqrt{\tau_s}},$$

$$Q_1^{R-}(v,z) = \frac{\nu_0}{\tilde{\mu}}((e^{\frac{2\tilde{\mu}(V_r-\theta)}{\tilde{\sigma}^2}} - 1)(\alpha + 2v) - \sum_{n=1}^{+\infty} \beta_n v_n^+(\sqrt{2}z)e^{-\sqrt{2n}v}) \tag{4.30}$$

$$Q_1^{R+}(v,z) = \frac{\nu_0}{\tilde{\mu}}(e^{\frac{2\tilde{\mu}(V_r-\theta)}{\tilde{\sigma}^2}}(\alpha + 2v) + 2z) \tag{4.31}$$

$$Q_1^{T}(x,z) = \frac{\nu_0}{\tilde{\mu}}\left(\alpha + 2x + 2z + \sum_{n=1}^{+\infty} \beta_n v_n^+(\sqrt{2}z)e^{-\sqrt{2n}x}\right), \tag{4.32}$$

where Q_1^{R-} (Q_1^{R+}) describes the p.d.f. in the boundary layer below (above) reset, $Q_1^T(x,z)$ describes the p.d.f. in the boundary layer below threshold, α and the β_ns are parameters given by equations A.45 and A.46, and the v_ns are sets of functions given in terms of Hermite polynomials in equation A.47.

Note that there are two components in the boundary solutions: the terms linear in v, x, and z match the outer solution close to reset (threshold), and the sum of exponentially decaying terms in x or v is needed to satisfy the boundary condition and vanish far from the boundaries. We show in Figure 4 an example of such a p.d.f. Note that contrary to the white noise regime, the probability density at threshold $P(\theta, z)$, integrated over z, is nonzero. This is an important feature that will qualitatively change the dynamical properties of this model, as we will see in section 5.

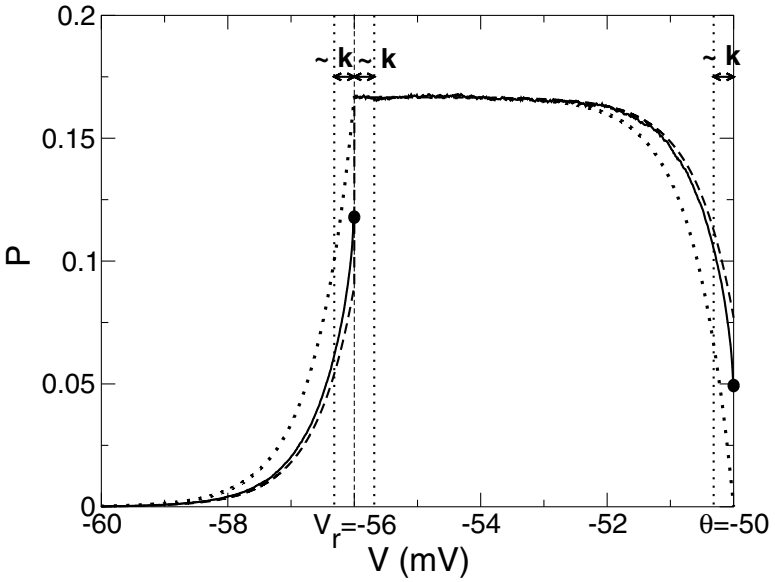

Figure 4: Stationary p.d.f. of the SIF neuron integrated over z for $\tau_s/\tau_e = 0.05$, $\tilde{\mu} = 1.25$ mV.ms^{-1}, and $\tilde{\sigma} = 1.25$ mV.ms$^{-\frac{1}{2}}$. Solid line: numerical simulation. Dashed line: outer solution, equations 4.26–4.29. Dotted line: p.d.f. for white noise. Black circles: value of P just below threshold, computed from equation 4.32 at $x = 0$, and just below reset, computed from equation 4.30 at $v = 0$. Note the good agreement between the analytical calculation (black dots) and the numerical simulations at threshold and reset potential. For colored noise, there is a finite fraction of neuron population near threshold.

4.2.4 The p.d.f. and Firing Rate of the LIF Neuron. The stationary firing rate is, up to first order in k,

$$\nu = \nu_0 - \sqrt{\frac{\tau_s}{\tau_m}} \frac{\alpha}{\tau_m 2\sqrt{\pi}} \frac{\Psi(\frac{\theta-\mu}{\sigma}) - \Psi(\frac{V_r-\mu}{\sigma})}{\left(\int_{\frac{V_r-\mu}{\sigma}}^{\frac{\theta-\mu}{\sigma}} \Psi(s)\, ds\right)^2}, \tag{4.33}$$

where $\Psi(s) = e^{s^2}(1 + \mathrm{erf}(s))$.

Up to first order in k, the result for the firing rate is compatible with the following simple expression:

$$\frac{1}{\nu} = \tau_m \sqrt{\pi} \int_{\frac{V_r-\mu}{\sigma} + \frac{\alpha}{2}\sqrt{\frac{\tau_s}{\tau_m}}}^{\frac{\theta-\mu}{\sigma} + \frac{\alpha}{2}\sqrt{\frac{\tau_s}{\tau_m}}} \Psi(s)\, ds.$$

Thus, the synaptic decay time effectively introduces an effective threshold $\theta + \sigma \frac{\alpha}{2}\sqrt{\frac{\tau_s}{\tau_m}}$ and an effective reset potential $V_r + \sigma \frac{\alpha}{2}\sqrt{\frac{\tau_s}{\tau_m}}$. Note that in Brunel and Sergi (1998), only the effective threshold appeared, due to the assumption made there.

We can also express the outer reduced probability density of the membrane potentials (the p.d.f. integrated over the synaptic current variable) by

$$P(V) = \frac{2\nu\tau_m}{\sigma} \exp\left(-\frac{(V-\mu)^2}{\sigma^2}\right) \begin{cases} \int_{\frac{V_r-\mu}{\sigma}+\frac{\alpha}{2}\sqrt{\frac{\tau_s}{\tau_m}}}^{\frac{\theta-\mu}{\sigma}+\frac{\alpha}{2}\sqrt{\frac{\tau_s}{\tau_m}}} \exp(s^2)\, ds & \text{if } V < V_r \\ \int_{\frac{V-\mu}{\sigma}}^{\frac{\theta-\mu}{\sigma}+\frac{\alpha}{2}\sqrt{\frac{\tau_s}{2\tau_m}}} \exp(s^2)\, ds & \text{if } V > V_r \end{cases}.$$

The boundary layer p.d.f.s turn out to be quite similar to the ones of the SIF. In particular, the threshold layer p.d.f. is, using the variable $x = \frac{\theta - V}{\sigma k}$, given by the same expression as the SIF equation, 4.32.

Note that again, the main difference with the white noise case is that colored noise introduces a finite probability density at firing threshold. This has important consequences for the dynamics, as we will see in the following.

5 Dynamical Response

In this section, we consider an oscillatory input given by

$$I_e(t) = \epsilon\mu\cos(\omega t). \tag{5.1}$$

The firing rate of the neuron is now driven by the oscillatory input. In the linear approximation, the firing rate is

$$\nu(t) = \nu[1 + \epsilon r(\omega)\cos(\omega t + \Phi(\omega)], \tag{5.2}$$

where $r(\omega)$ is the relative amplitude of the firing-rate modulation and $\Phi(\omega)$ is the phase lag.

Our technique to solve this problem is again to solve the Fokker-Planck equation associated with the system of stochastic equations, using an expansion of the p.d.f. and the instantaneous firing rate at the first order in ϵ.

The dynamics of the leaky IF neuron in the presence of white noise has already been discussed by Brunel and Hakim (1999) and Lindner and Schimansky-Geier (2001) (see also Melnikov 1993 for the dynamics of a related system). We include here the results for completeness. Some of the results for synaptic colored noise appear in Brunel et al. (2001).

5.1 White Noise. The problem can be solved exactly when $\tau_s = 0$. The stochastic equation, 3.3, is equivalent to the Fokker-Planck equation for the

probability density $\mathcal{P}(V,t)$ (using complex input to simplify the calculations)

$$\tau_m \frac{\partial \mathcal{P}_0}{\partial t} = \frac{\sigma^2}{2}\frac{\partial^2 \mathcal{P}_0}{\partial V^2} - \frac{\partial}{\partial V}[f(V) + \mu(1+\epsilon e^{i\omega t})]\mathcal{P}_0, \tag{5.3}$$

and the boundary conditions are now

$$\mathcal{P}_0(\theta,t) = 0 \tag{5.4}$$

$$\frac{\partial \mathcal{P}_0}{\partial V}(\theta,t) = -\frac{2\nu(t)\tau_m}{\sigma^2} \tag{5.5}$$

$$\mathcal{P}_0(V_{r+},t) - \mathcal{P}_0(V_{r-},t) = 0 \tag{5.6}$$

$$\frac{\partial \mathcal{P}_0}{\partial V}(V_{r+},t)) - \frac{\partial \mathcal{P}_0}{\partial V}(V_{r-},t) = -\frac{2\nu(t)\tau_m}{\sigma^2}. \tag{5.7}$$

Our strategy is to solve equation 5.3 with its associated boundary conditions using an expansion in the small parameter ϵ. Thus, we write

$$\nu(t) = \nu_0[1 + \epsilon \hat{n}_0(\omega)e^{i\omega t} + O(\epsilon^2)] \tag{5.8}$$

$$\mathcal{P}_0(V,t) = P_0(V) + \epsilon e^{i\omega t}\hat{P}_0(V,\omega) + O(\epsilon^2), \tag{5.9}$$

where $\hat{n}_0(\omega) = r_0(\omega)\exp(i\Phi(\omega))$ and $\hat{P}_0(V,\omega)$ are complex quantities describing the oscillatory component at the frequency input ω of the instantaneous firing rate and the voltage probability density.

The zeroth order in ϵ gives the stationary response obtained in section 4. At the first order, we have

$$i\omega\tau_m\hat{P}_0 = \frac{\sigma^2}{2}\frac{\partial^2 \hat{P}_0}{\partial V^2} - \frac{\partial}{\partial V}[f(V)+\mu]\hat{P}_0 - \mu\frac{dP_0}{dV}, \tag{5.10}$$

with the boundary conditions

$$\begin{aligned}
\hat{P}_0(\theta,\omega) &= 0 \\
\frac{\partial \hat{P}_0}{dV}(\theta,\omega) &= -\frac{2\hat{n}_0(\omega)\nu_0\tau_m}{\sigma^2} \\
\hat{P}_0(V_{r+},\omega) - \hat{P}_0(V_{r-},\omega) &= 0 \\
\frac{\partial \hat{P}_0}{dV}(V_{r+},\omega)) - \frac{\partial \hat{P}_0}{dV}(V_{r-},\omega) &= -\frac{2\hat{n}_0(\omega)\nu_0\tau_m}{\sigma^2}.
\end{aligned} \tag{5.11}$$

The response of the SIF neuron is given by (see details in Abbott & van Vreeswijk, 1993, and section B.1)

$$\begin{aligned}
\hat{P}_0(V,\omega) = \frac{\nu_0}{i\omega}\Bigg[& e^{\frac{2\tilde{\mu}(V-V_\theta)}{\tilde{\sigma}^2}} - e^{r_+(\omega)\frac{2\tilde{\mu}(V-V_\theta)}{\tilde{\sigma}^2}} - \Theta(V_r - V) \\
& \times\left(e^{\frac{2\tilde{\mu}(V-V_r)}{\tilde{\sigma}^2}} - e^{r_+(\omega)\frac{2\tilde{\mu}(V-V_r)}{\tilde{\sigma}^2}}\right)\Bigg],
\end{aligned} \tag{5.12}$$

with

$$r_+(\omega) = \frac{1 + \sqrt{1 + 2i\tau_e\omega}}{2}, \tag{5.13}$$

where τ_e is given by equation 4.28, and

$$\hat{n}_0(\omega) = \frac{\sqrt{1 + 2i\tau_e\omega} - 1}{i\tau_e\omega}. \tag{5.14}$$

The neuron reproduces inputs at frequencies lower than $\frac{1}{\tau_e}$ with little attenuation and a small phase lag. Inputs at high frequencies are attenuated by a factor $\sqrt{\frac{2}{\tau_e\omega}}$, with a phase lag that tends to $-\frac{\pi}{4}$. The amplitude and phase of $\hat{n}_0(\omega)$ are shown in figure 6A.

The response of the LIF neuron is (Brunel & Hakim, 1999; Brunel et al., 2001)

$$\hat{n}_0(\omega) = \frac{\mu}{\sigma(1 + i\omega\tau_m)} \frac{\frac{\partial U}{\partial y}(y_\theta, \omega) - \frac{\partial U}{\partial y}(y_r, \omega)}{U(y_\theta, \omega) - U(y_r, \omega)}, \tag{5.15}$$

where $y_\theta = \frac{\theta - \mu}{\sigma}$, $y_r = \frac{V_r - \mu}{\sigma}$, and U is given in terms of combinations of hypergeometric functions (Abramowitz & Stegun, 1970):

$$\begin{aligned} U(y, \omega) = {} & \frac{e^{y^2}}{\Gamma\left(\frac{1 + i\omega\tau_m}{2}\right)} M\left(\frac{1 - i\omega\tau_m}{2}, \frac{1}{2}, -y^2\right) \\ & + \frac{2ye^{y^2}}{\Gamma\left(\frac{i\omega\tau_m}{2}\right)} M\left(1 - \frac{i\omega\tau_m}{2}, \frac{3}{2}, -y^2\right). \end{aligned} \tag{5.16}$$

In the high-frequency limit,

$$\hat{n}_0(\omega) \sim \sqrt{\frac{2}{i\omega\tau_e}}. \tag{5.17}$$

This is the same asymptotic behavior as observed for the SIF neuron.

5.2 Synaptic Noise: Analytical Calculations. We now introduce the relaxation time τ_s of the synaptic current. We proceed along the lines of section 4.2.2. $\mathcal{P}(V, I_s, t)$, the probability density of finding the neuron at potential V and synaptic current I_s at time t, and $\nu(t)$, the instantaneous firing rate, are expanded in k (see equation 4.24). There are now two small parameters, k and ϵ. The goal of this section is to obtain the first order in both parameters, that is, in $k\epsilon$.

The stochastic system we have to solve is given by equations 3.5 and 3.6. As in the computation of the stationary p.d.f., we prefer to use a synaptic variable that keeps a finite variance in the small synaptic time limit. Thus, we use here

$$z = \frac{k}{\sigma}(I_s(t) + f(\theta) + \epsilon\mu e^{i\omega t}), \tag{5.18}$$

which describes the input of the neuron (synaptic and external). Moreover, since z represents the complete input of the neuron, it simplifies the description of the boundary conditions.

The FP equation associated with equations 3.5 and 3.6 is

$$\frac{\partial \mathcal{P}}{\partial t} = -\frac{\partial J_V}{\partial V} - \frac{\partial J_z}{\partial z} \tag{5.19}$$

$$J_V = \frac{1}{\tau_m}\left(f(V) - f(\theta) + \frac{\sigma z}{k}\right)\mathcal{P} \tag{5.20}$$

$$J_z = -\frac{1}{k^2\tau_m}\left[\frac{1}{2}\frac{\partial \mathcal{P}}{\partial z} + z\mathcal{P}\right] + \frac{1}{k\tau_m}\left(\frac{f(\theta)+\mu}{\sigma} + \epsilon\frac{\mu}{\sigma}(1 + k^2 i\omega\tau_m)e^{i\omega t}\right)\mathcal{P}. \tag{5.21}$$

As in equation 4.17, the instantaneous firing rate is given by the probability flux in the z direction through θ integrated over z,

$$\nu(t) = \int_{-\infty}^{+\infty} J_V(\theta, z, t)\, dz, \tag{5.22}$$

where $J_V(\theta, z, t)$ is given by

$$J_V(\theta, z, t) = \frac{\sigma z}{k\tau_m}\mathcal{P}(\theta, z, t). \tag{5.23}$$

Note that due to the factor $\frac{1}{k}$ in the expression of $J_V(\theta, z, t)$, we have to expand $\mathcal{P}$ to the second order in k to obtain the first-order correction to the instantaneous firing rate.

The boundary conditions at firing threshold and reset are again (compare with equation 4.18),

$$J_V(\theta, z, t) = 0, \quad \text{for} \quad z < 0 \tag{5.24}$$

$$J_V(V_r^+, z, t) = J_V(V_r^-, z, t), \quad \text{for} \quad z < 0. \tag{5.25}$$

The other boundary conditions at $z = \pm\infty$ or $V = -\infty$ are the same as in the case without synaptic relaxation and hold for both P and $\hat{P}$.

At first order in ϵ, equation 5.19 gives

$$k^2 i\omega\tau_m \hat{P} = \frac{1}{2}\frac{\partial^2 \hat{P}}{\partial z^2} + \frac{\partial(z\hat{P})}{\partial z} - k\frac{\partial}{\partial z}\left[\left(\frac{f(\theta)+\mu}{\sigma}\right)\hat{P}\right] - k^2\frac{\partial}{\partial V}\left[\left(f(V)-f(\theta)+\frac{\sigma z}{k}\right)\hat{P}\right] - k\frac{\mu}{\sigma}(1+k^2 i\omega\tau_m)\frac{dP}{dz}. \tag{5.26}$$

We again solve the equation by expanding the density probability in k. We note

$$P = P_0 + kP_1 + k^2 P_2 + \cdots \tag{5.27}$$

$$\hat{P} = \hat{P}_0 + k\hat{P}_1 + k^2\hat{P}_2 + \cdots \tag{5.28}$$

$$\nu = \nu_0 + k\nu_1 + \cdots \tag{5.29}$$

$$\hat{n} = \hat{n}_0 + k\hat{n}_1 + k^2\hat{n}_2 + \cdots \tag{5.30}$$

Analytical solutions can be found in two opposite limits: at low frequencies $\omega \sim \frac{1}{\tau_e}$ and at high frequencies $\omega \gg \frac{1}{\tau_s}$. To connect these two limits, we resort to numerical solutions:

Low-frequency regime. The solution of the problem is very similar to the stationary case (see section 4.2.2). The details of the computation can be found in section B.1. We find that in this regime, the correction at the first order in k of the firing-rate oscillation amplitude vanishes for both models of neurons. Thus, the synaptic decay time has little effect on the dynamics of the firing probability at low frequencies.

High-frequency regime. When $\omega \gg \frac{1}{\tau_s}$, equation 5.26 simplifies to

$$\hat{P} = -k\frac{\mu}{\sigma}\frac{dP}{dz} + o\left(\frac{1}{\sqrt{\omega\tau_s}}\right). \tag{5.31}$$

Thus, the high-frequency modulation of the probability density is related in a simple way to the derivative with respect to the current variable of the stationary probability density.

The firing probability is

$$\nu(t) = \int_{-\infty}^{+\infty} J_V(\theta, z, t)\, dz = \frac{\sigma}{k\tau_m}\int_{-\infty}^{+\infty} z(P(\theta, z) + \epsilon\hat{P}(\theta, z)e^{i\omega t})\, dz. \tag{5.32}$$

We already know the contribution of the term at the order zero in ϵ (see section 4.2). According to equation 5.31, to obtain the limit at large ω for the

first order in k of $\hat{n}$, we need to compute

$$-\int_{-\infty}^{+\infty} z\frac{dP_1}{dz}(\theta, z)\,dz = \int_{-\infty}^{+\infty} P_1(\theta, z)\,dz. \tag{5.33}$$

Using equations 5.32 and 4.32, we obtain for high-input frequency modulation

$$\hat{n} = k\frac{\mu}{\sigma}A + O(k^2) = Ak' + O(k^2), \tag{5.34}$$

where we have defined

$$k' = k\frac{\mu}{\sigma} = \sqrt{\frac{\tau_s\tilde{\mu}^2}{\tilde{\sigma}^2}} = \sqrt{\frac{\tau_s}{\tau_e}},$$

where τ_e is given in equation 4.28, and

$$A = \sqrt{2}\left|\zeta\left(\frac{1}{2}\right)\right| - \frac{1}{\sqrt{2}}\sum_n \frac{N(\sqrt{n})n^{\frac{n-1}{2}}e^{-\frac{n}{2}}}{n!} \simeq 1.3238. \tag{5.35}$$

ζ is Riemann's zeta function, and $N(\sqrt{n})$ is given by equation A.48.

We see that introducing the synaptic relaxation time τ_s drastically changes the behavior of the neuron with respect to high-frequency components in the inputs (larger than $1/\tau_s$). In this regime, the amplitude of the modulation of the output firing rate is proportional to $\sqrt{\tau_s/\tau_e}$, and there is no phase shift.

Qualitatively, this behavior can be understood from equation 5.33. It shows that the firing-rate modulation in this regime is proportional to the cumulative probability density at the threshold. We have seen in section 4.2.3 that there is a finite fraction of the neuron population close to the threshold as soon as the synaptic decay time is finite. This finite fraction is responsible for the instantaneous response to fast changes in the inputs.

5.2.1 The Large Synaptic Time, High-Frequency Limit. The large synaptic time limit corresponds to the limit in which noise vanishes. The noiseless dynamical response was computed by Knight (1972).

SIF neuron. In the absence of noise, the SIF neuron reproduces exactly the synatic input:

$$\lim_{\omega\to+\infty,k\to+\infty} \hat{n}(\omega) = 1. \tag{5.36}$$

LIF neuron. Taking the high-frequency limit, we find after some algebra a simple expression for the high-frequency limit of the response:

$$\lim_{\omega\to+\infty,k\to+\infty} \hat{n}(\omega) = \frac{\mu}{\mu-\theta}. \tag{5.37}$$

Note that the noiseless high-frequency response is now in general different from the low-frequency one, contrary to the SIF neuron.

5.3 Synaptic Noise: Numerical Simulations. We performed numerical simulations to obtain the neuronal response function in the whole input frequency range. The stochastic equations were simulated with a Euler method for different values of the parameters. We used a neuron with a reset potential $V_r = -56$ mV and a firing threshold $\theta = -50$ mV. The integration time step was chosen to be small compared to the time constants of the problem (τ_s, $1/\nu_0$ and $1/\omega$).

5.3.1 SIF Neuron. The parameters characterizing the input, $\tilde{\sigma}$ and $\tilde{\mu}$, were held constant, respectively equal to $\tilde{\sigma} = 1.25$ mV.ms$^{-\frac{1}{2}}$ and $\tilde{\mu} = 0.28$ mV.ms^{-1}, which gives $\tau_e = 20$ ms and $\nu_0 = 46.6$ Hz. In this case, we found that the dependence of the gain function of the neuron on ϵ is linear even for large-input oscillation amplitudes. Thus, we usually choose $\epsilon = 0.5$ in the simulations.

5.3.2 LIF Neuron. Since the stationary firing rate of the LIF neuron depends on τ_s, all curves were plotted keeping the mean firing rate constant. To keep the firing rate constant, the mean input μ was varied.

5.3.3 High-Frequency limit versus k. The high-frequency limit of the modulation amplitude was determined by choosing $\omega = 10^5$ Hz. This value was chosen because it is much larger than the inverse of the synaptic decay times for any τ_s for which simulations were made. The neuronal response function is shown in Figure 5. The graphics show a linear dependence for small values of k.

For the SIF neuron (see Figure 5A), a fit of the curve (computed at $\omega = 10^5$ Hz here) in the small k' region (from $k' = 0.1$ to $k' = 1$) by a quadratic function gives

$$r(\omega = 10^5 \text{ Hz}, k) \simeq 1.32 \pm 0.02k' - 0.46 \pm 0.05k'^2, \tag{5.38}$$

which is in good agreement with the analytical result, equation 5.35. Moreover, we find that the full curve (from $k' = 0$ to $k' = 7$) is well described by the following function,

$$r_{HF}(\tau_s) = \lim_{\omega \to \infty} r(\omega, \tau_s) \simeq \frac{1 - e^{-2Ak'}}{1 + e^{-ak'}}, \tag{5.39}$$

where $A \simeq 1.32$ is given by equation 5.35 and a one-parameter fit gives $a = 2.2 \pm 0.1$. The function on the right-hand side of equation 5.39 is the simplest function we could find that has the behavior predicted by theory for small k (i.e., $\sim Ak$), has the correct behavior at large k (see equation 5.36), and provides a good fit of all the simulation data.

For the LIF neuron (see Figure 5B), we find that the behavior of the high-frequency-modulation amplitude versus k is again well described by the

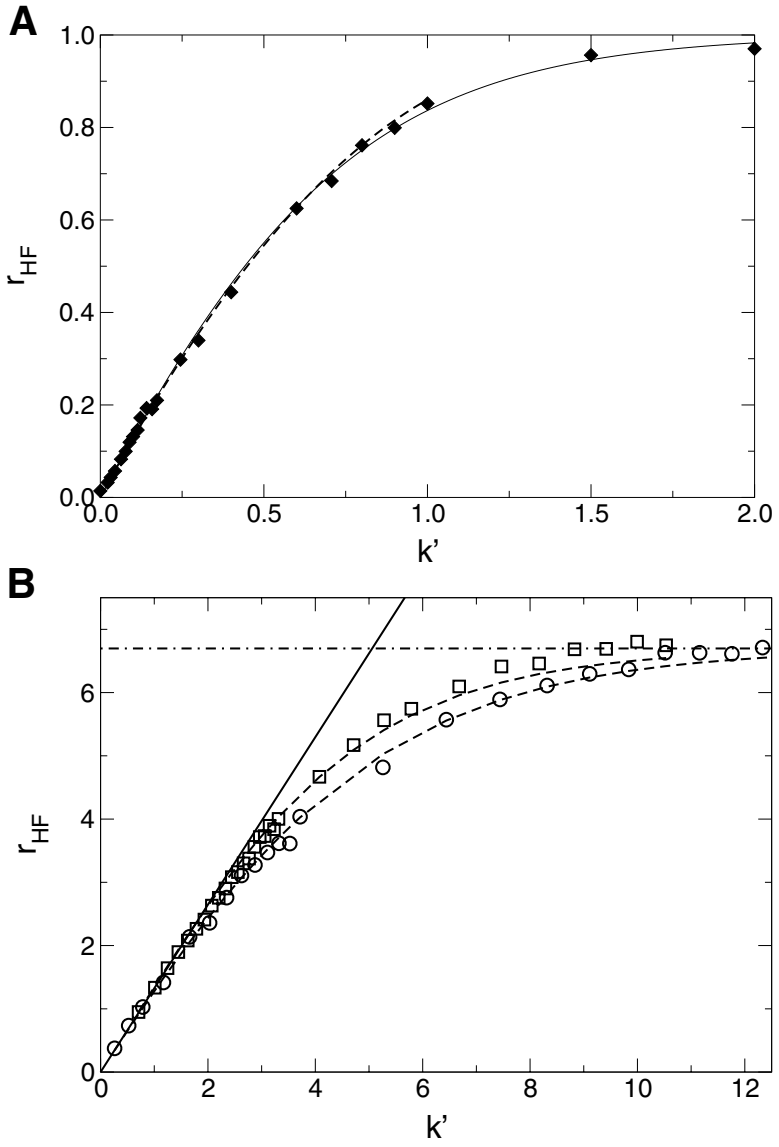

Figure 5: High-frequency limit of the gain (estimated at $\omega = 10^5$ Hz) versus k'. (A) SIF neuron with $\tau_e = 20$ ms. Note the linear relation for small values of k'. Solid line: fit given by equation 5.39, dashed line: fit for small k' given by equation 5.38. (B) LIF neuron with $\nu = 50$ Hz, $\tau_m = 20$ ms, $\epsilon\mu = 2$ mV kept constant, and two values of σ: $\sigma = 1$ mV (○), 5 mV (□). The solid line is the prediction of the theory, equation 5.35, with a slope equal to 1.3238. We also show the fits given by equation 5.40 (dashed lines) and the asymptotic limit at low noise and high frequencies given by equation 5.37 (dotted-dashed line).

Table 1: Values Obtained by Fitting the Response Module with Equation 5.41.

τ_s(ms)	$l(\tau_s)$	b	c	p
1.8	0.349 ± 2	0.10 ± 1	0.14 ± 15	3.6 ± 10
3.2	0.459 ± 1	0.099 ± 2	0.004 ± 4	5.9 ± 9
7.2	0.624 ± 2	0.111 ± 9	0.019 ± 31	5.5 ± 16
12.8	0.747 ± 1	0.110 ± 5	0.07 ± 3	5.2 ± 6
16.2	0.793 ± 2	0.102 ± 8	0.06 ± 6	5.2 ± 14

Note: The error bars are on the last digits.

following function,

$$r_{HF}(\tau_s) = B\frac{1 - e^{-\frac{2A}{B}k'}}{1 + e^{-c(\nu,\sigma)k'}}, \tag{5.40}$$

with A given by equation 5.35, B by equation 5.37, and c determined by a one-parameter fit. Contrary to the SIF, this parameter depends on ν and σ. For example, $c(\nu = 50\text{ Hz}, \sigma = 1\text{ mV}) = 0.34 \pm 0.01$ and $c(\nu = 50\text{ Hz}, \sigma = 5\text{ mV}) = 0.47 \pm 0.01$. These fits are sketched in Figure 5B.

5.3.4 Response vs. Frequency. In Figure 6, we show the amplitude and phase of the firing-rate modulation as a function of the frequency of the modulation in the input for different values of τ_s. Simulations confirm the high-frequency behavior obtained in the analysis, as we showed in Figure 5. The high-frequency limit of the response is finite, and the phase tends to 0 for any nonzero τ_s. Simulations also confirm that the behavior at low frequencies is affected very little by the synaptic filtering.

In the SIF neuron case in the high-frequency regime, simulation results indicate that the modulation amplitude is well described by a function of the form $r_{HF}(\tau_s) + \frac{b}{\omega\tau_s}$, where r_{HF} is the high-frequency limit of the response. The low-frequency regime is given by the white noise gain function $\hat{n}(\omega, 0)$. Then it is natural to interpolate between these two regimes by a sigmoid function. We find that the complete amplitude response function can be well described by

$$r(\omega, \tau_s) = r(\omega, 0) + \frac{(\omega\tau_s)^p}{c + (\omega\tau_s)^p}\left(r_{HF}(\tau_s) + \frac{b}{\omega\tau_s} - r(\omega, 0)\right). \tag{5.41}$$

The values of $r_{HF}(\tau_s)$ obtained by fitting the curves over the whole range of frequency are the same as the values obtained with a fit only in the high-frequency range. We give the results of fits over the whole parameters for different values of τ_s (note the error bars are on the last digits) in Table 1. b, c, and p are essentially independent of τ_s, and we show two examples of these fits in the left panel of Figure 7 with $b = 0.1$, $c = 0.06$, and $p = 5$.

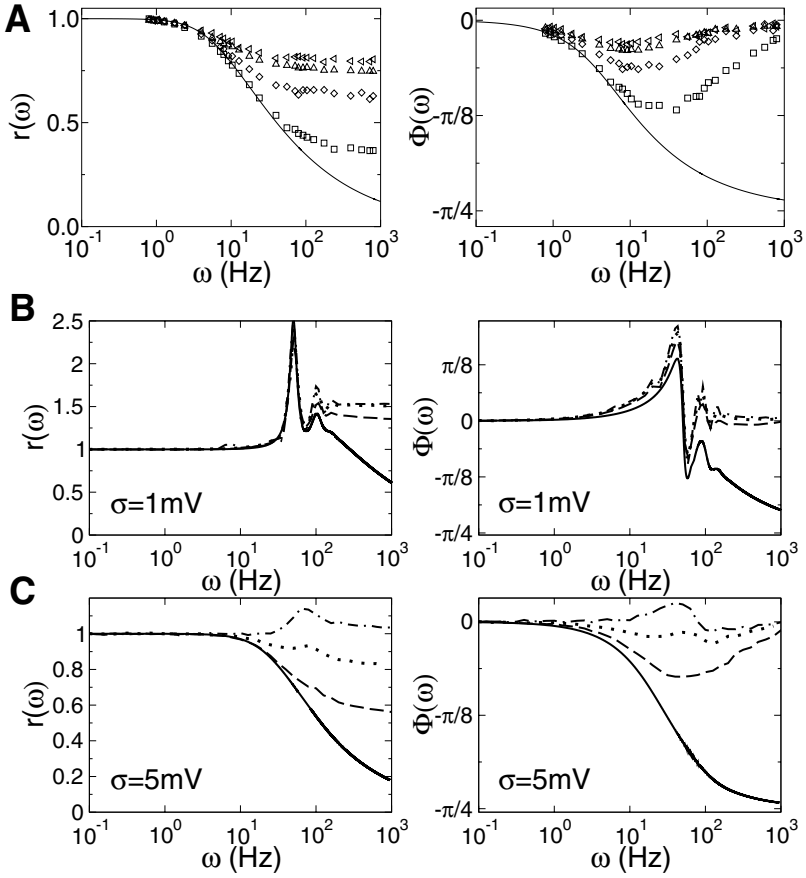

Figure 6: Numerical simulations of the amplitude and phase of the response function for different values of τ_s. (A) SIF neuron: $\tau_s = 0$ ms (solid line—amplitude of equation 5.14), 1.8 ms (□), 7.2 ms (◇), 12.8 ms (△), 16.2 ms (◁). (B) Low noise. (C) High noise. LIF neuron, response normalized to 1 at $\omega = 0.1$ Hz with $\nu_0 = 50$ Hz and $\tau_m = 20$ ms. $\tau_s = 0$ ms—white noise (solid line), $\tau_s = 2$ ms (dashed line), 5 ms (dotted line), 10 ms (dot-dashed line). In all cases we have $\nu_0 = 50$ Hz and $\tau_m = 20$ ms. The size of the error bars is of the order of the size of the symbols.

Similarly, the phase lag Φ can be well described by

$$\Phi(\omega, \tau_s) = \Phi(\omega, 0)\left(1 - \frac{(\omega\tau_s)^q}{a + (\omega\tau_s)^q}\right). \tag{5.42}$$

We give the results of fits over the whole parameters for different values of τ_s in Table 2.

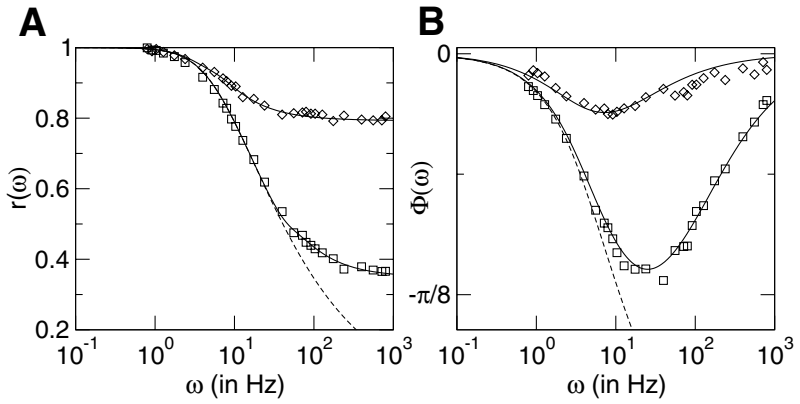

Figure 7: Fits of the gain function of the SIF neuron for different values of τ_s: $\tau_s = 1.8$ ms (□), $\tau_s = 16.2$ ms (◇). (A) Amplitude. (B) Phase. The solid lines are equation 5.41 with $b = 0.1$, $c = 0.06$, and $p = 5$ (amplitude), and equation 5.42, with $p = 0.8$ and the value of a obtained by the fit given in Table 2 (phase). The dashed line is the white noise neuronal response.

Table 2: Values Obtained by Fitting the Response Phase Lag with Equation 5.43.

τ_s(ms)	a	q
1.8	0.82 ± 2	0.87 ± 3
3.2	0.698 ± 8	0.87 ± 1
7.2	0.56 ± 2	0.81 ± 2
12.8	0.408 ± 8	0.70 ± 1
16.2	0.34 ± 1	0.59 ± 2

Note: The error bars are on the last digits.

The parameter q is also essentially independent of τ_s over a large interval. For τ_s of order τ_e or larger, the phase becomes close to 0 for all input frequencies. Examples are shown in the right panel of Figure 7. When $\tau_s = 16$ ms, the phase lag is less than $\pi/30$ for any input frequency.

Simulations of the LIF response are plotted in Figure 6 as a function of frequency. In a small noise case ($\sigma = 1$ mV, in Figure 6B), there are pronounced resonant peaks at frequencies equal to or multiples of the background firing rate. In a large noise case ($\sigma = 5$mV in Figure 6C), the resonances have almost disappeared. It shows that as it has been found in the analytical calculation, the low-frequency regime is not affected by the synaptic filtering. In particular, the resonant peaks in the small noise regime are still present. Moreover, we can note that in the small noise case, the high-frequency response of the neuron is greater than its low-frequency response with realistic

synaptic time constants. The response in the large noise case is very similar to the curve response of the SIF neuron. An important difference is that the resonant peaks appear again when τ_s increases. This is to be expected in the light of the results of Knight (1972), who showed that without noise (infinite τ_s limit), the LIF neuron response has infinite resonant peaks.

5.4 Synaptic Currents with Rise Time. When a rise time is introduced, the FP equation becomes three-dimensional. Tackling such a problem analytically is beyond the scope of this article; thus, we resorted to numerical simulations. We simulated equations 2.1, 2.8, and 2.9 using the diffusion approximation, 3.1. We used the same method as described in section 5.3 and kept the same value of μ and σ to compare with the case without rise time, $\tau_r = 0$.

The simulations show that the important parameter controlling the response is the sum of rise and decay times, $\tau_r + \tau_s$. It shows that the system behaves essentially like a neuron with instantaneous rise and a decay time constant $\tau_s' = \tau_r + \tau_s$. Figure 8 shows results of simulations with different values of τ_r and τ_s keeping their sum τ_s' fixed.

This result can be understood by the following simple argument. One of the factors controlling the effects of noise on neuronal dynamics is the standard deviation of the synaptic inputs I_s. When the neuron has no rise time, this standard deviation is proportional to $\sqrt{\tau_m/\tau_s} = 1/k$ (see equation 4.25). If we take into account the rise time, we find

$$\sqrt{\Delta {I_s}^2} \sim \sqrt{\frac{\tau_m}{\tau_r + \tau_s}}. \tag{5.43}$$

Thus, it is natural to define an effective relaxation time $\tau_s' = \tau_r + \tau_s$. As shown in Figure 8, this relationship describes particularly well the numerical results for all input frequencies.

5.5 Two or More Distinct Synaptic Currents. Synaptic currents in the nervous system have different temporal dynamics due to the variety of the receptors giving rise to such currents. We consider here the case of two types of synaptic currents with decay times τ_{s_1} and τ_{s_2}. The variance of the input noise due to these synaptic currents is noted σ_1 and σ_2. The neuron is described by the system of equations,

$$\tau_m \frac{dV}{dt} = f(V) + I_{s_1}(t) + I_{s_2}(t) + \epsilon\mu e^{i\omega t} \tag{5.44}$$

$$\tau_{s_1} \frac{dI_{s_1}}{dt} = -I_{s_1}(t) + \mu_1 + \sigma_1\sqrt{\tau_m}\eta_1(t) \tag{5.45}$$

$$\tau_{s_2} \frac{dI_{s_2}}{dt} = -I_{s_2}(t) + \mu_2 + \sigma_2\sqrt{\tau_m}\eta_2(t), \tag{5.46}$$

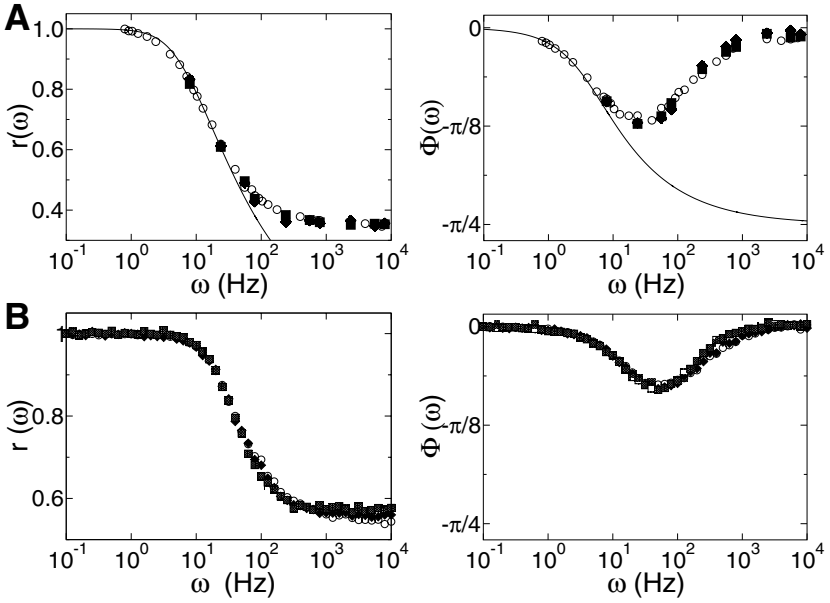

Figure 8: Amplitude and phase of the gain function of the neuron with different values of τ_r and τ_s. Here, we keep $\tau_r + \tau_s$ constant; the curves are almost superimposed. (A) SIF neuron: ○: $\tau_s = 1.8$ ms, $\tau_r = 0$ ms. □: $\tau_s = 1.6$ ms, $\tau_r = 0.2$ ms. ◇: $\tau_s = \tau_r = 0.9$ ms. The solid line corresponds to the white noise regime. (B) LIF neuron, with $\nu_0 = 50$ Hz and $\sigma = 5$ mV, response normalized to 1 at $\omega = 0.1$ Hz: $\tau_s = 2$ ms and $\tau_r = 0$ ms (○), $\tau_s = 1.8$ ms and $\tau_r = 0.2$ ms (◇), $\tau_s = \tau_r = 1$ ms (□). Note that the size of the error bars is of the order of the size of the symbols.

where $\langle \eta_i(t) \rangle = 0$ and $\langle \eta_i(t)\eta_i(t') \rangle = \delta(t - t')$. We also note $\tilde{\sigma}_i \sqrt{\tau}_m = \sigma_i$, $\tilde{\mu}_i \tau_m = \mu_i$.

Numerical simulations were performed as in section 5.3. We used $\mu_1 + \mu_2 = \mu$ and $\sigma_1^2 + \sigma_2^2 = \sigma^2$ with μ and σ as in the previous simulations in order to compare the results in the small τ_{s_1} and/or τ_{s_2} limits. We also chose $\tau_{s_1} > \tau_{s_2}$. Results are shown in Figure 9. In most cases, we can completely describe the response with an effective relaxation time given by

$$\tau_s' = \frac{\sigma_1^2 + \sigma_2^2}{\frac{\sigma_1^2}{\tau_{s_1}} + \frac{\sigma_2^2}{\tau_{s_2}}} \quad \text{or} \quad \frac{\sigma_1^2 + \sigma_2^2}{\tau_s'} = \frac{\sigma_1^2}{\tau_{s_1}} + \frac{\sigma_2^2}{\tau_{s_2}}. \tag{5.47}$$

An intuitive understanding of this result can again be obtained with the same argument as in section 5.4. The standard deviation of I_s is indeed

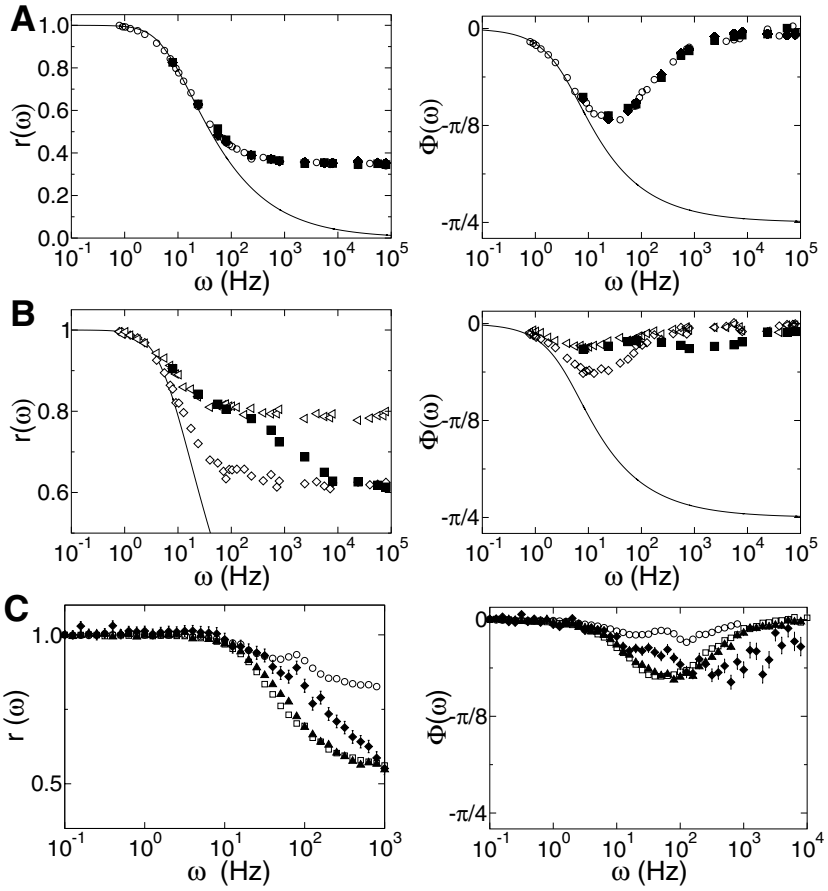

Figure 9: Amplitude and phase of the gain function of the neuron for different values of τ_{s_1}, τ_{s_2}, σ_1, and σ_2. We keep constant the effective relaxation time τ_s' given by equation 5.47. (A) SIF neuron: ○: single synaptic current, $\tau_s = 1.8$ ms. □: $\tau_{s_1} = 20$ ms, $\tau_{s_2} = 0.39$ ms, $\tilde{\sigma}_1 = 1.12$ mV.ms$^{-\frac{1}{2}}$, and $\tilde{\sigma}_2 = 0.56$ mV.ms$^{-\frac{1}{2}}$. ◇: $\tau_{s_1} = 20$ ms, $\tau_{s_2} = 1.72$ ms, $\tilde{\sigma}_1 = 0.28$ mV.ms$^{-\frac{1}{2}}$, and $\tilde{\sigma}_2 = 1.22$ mV.ms$^{-\frac{1}{2}}$. (B) SIF neuron, crossover with $\tau_{s_1} \gg \tau_{s_2}$ and a very unbalanced noise case. Square: $\tau_{s_1} = 16.2$ ms, $\tau_{s_2} = 0.041$ ms, $\tilde{\sigma}_1 = 1.248$ mV.ms$^{-\frac{1}{2}}$, and $\tilde{\sigma}_2 = 0.07$ mV.ms$^{-\frac{1}{2}}$. We show here the curves with only one synaptic current with $\tau_s = 16.2$ ms (△) and $\tau_s = 7.2$ ms (◇), to highlight the crossover around $\omega \sim \frac{1}{\tau_{s_2}}$. (C) LIF neuron with $\nu_0 = 50$ Hz and $\tau_s' = 2$ ms, response normalized to 1 at $\omega = 0.1$ Hz: normal case: $\tau_{s_1} = 5$ ms, $\sigma_1 = 3.5$ mV and $\tau_{s_2} = 1.25$ ms, $\sigma_2 = 3.5$ mV (△); extreme case: $\tau_{s_1} = 5$ ms, $\sigma_1 = 4.9$ mV and $\tau_{s_2} = 0.13$ ms, $\sigma_2 = 1$ mV (◇). We also show the curves with a single synaptic current $\sigma = 5$ mV and $\tau_s = 5$ ms (○) and $\tau_s = 2$ ms (□). Error bars when not visible are of the order of the size of the symbols.

proportional to

$$\sqrt{\Delta^2 I_s} \sim \sqrt{\frac{\tau_m}{\tau_s'}}, \tag{5.48}$$

with τ_s' given by equation 5.47. Numerical simulations indicate that this value of τ_s' gives a very good estimate of the high-frequency limit.

If relaxation times are different by at least one order of magnitude and the variance of the noise is mostly concentrated on the slower synapses, we start to see differences from the simple picture governed by the single effective time. For input frequencies around $\frac{1}{\tau_{s_1}}$, the neuron feels as if all the noise was filtered with the slower relaxation time τ_{s_1}. Thus, the response is as if only this current was present. Then, for input frequencies around $\frac{1}{\tau_{s_2}}$, the neuron starts to feel the faster noise due to synaptic filtering with time constant τ_{s_2}. There is a crossover of the response function to a response governed by the effective synaptic decay time τ_s'. Thus, at high frequencies, we recover the response of a neuron with only one type of synaptic input and $\tau_s = \tau_s'$. Examples of this extreme case are shown in Figures 9B and 9C.

These arguments can be generalized to an arbitrary number of synaptic currents. In general, the response will be simply described by an effective decay time equal to

$$\tau_s' = \left(\sum_i \sigma_i^2\right)\left(\sum_i \frac{\sigma_i^2}{\tau_i}\right)^{-1}. \tag{5.49}$$

When there is a large gap between two sets of time constants, the response function of the neuron will experience a crossover at frequencies of the order of this gap. For frequencies lower than the crossover frequencies, the response of the neuron will be governed by an effective decay time given by equation 5.49, where the sums take into account only the slowest currents. For higher frequencies, the response of the neuron will be governed by the effective time constant taking into account all the currents. This scenario can be easily generalized to several large gaps between sets of time constants, where several crossovers show up.

6 Discussion

We have studied the influence of the filtering of noise by realistic synaptic dynamics on the dynamics of the instantaneous firing rate of IF neurons. Brunel et al. (2001) showed that filtering of noise with a finite synaptic time constant leads to a finite high-frequency limit of the response, and hence to an instantaneous component of the response of the instantaneous firing rate to any input. In this article, we first presented a detailed description of analytical methods that lead to results given in Brunel et al. (2001) on the high limit frequency of the neuronal response.

In particular, we presented the joint p.d.f. of voltage and synaptic current up to first order in k for both neuronal models and the link between the properties of the p.d.f. at threshold and the high-frequency response. Then we proceeded to investigate extensions of this result, mostly through numerical simulations:

- Characterization of low- and intermediate-input frequency regimes
- Characterization of the high-frequency response at all synaptic times τ_s
- Extension of these results to more realistic biological conditions, including either a rise time of postsynaptic currents or the presence of different types of synaptic receptors

Our calculations show that the probability density of the membrane potential is finite and of order $\sqrt{\tau_s/\tau_e}$ at the firing threshold, for both types of IF neuron models. When $\tau_s > 0$, the linear dynamical response of the IF neuron remains finite in the high-frequency limit, with no phase lag. This high-frequency behavior is intimately related to the finite probability density at firing threshold. An intuitive interpretation of this result is that when the probability to be at threshold is finite, there is an instantaneous component to the response of the firing probability to arbitrarily fast variations in input currents. In turn, the fact that the probability at threshold is finite is related to the fact that with a finite synaptic time constant, there is no diffusive term in the probability current going through threshold, contrarily to the white noise case, for which we get a $1/\sqrt{i\omega\tau_e}$ attenuation at high frequencies (Brunel & Hakim, 1999; Brunel et al., 2001). Numerical simulations allowed us to characterize the response function of the neuron at intermediate frequencies. For the simplest IF neuron, we found empirically compact descriptions of the response (for both amplitude and phase), which show that the crossover between the low- and high-frequency regime occurs at input frequencies of the order of $1/\tau_s$. More realistic synaptic current dynamics have been investigated. The introduction of a rise time τ_r does not change qualitatively the neuronal response. We showed how an effective relaxation time $\tau_s' = \tau_s + \tau_r$ can describe well the neuron response at all frequencies for both the simplest and leaky IF neuron models. In the case of several synaptic currents with different relaxation times, we defined again an effective relaxation time that describes well the high-input frequency regime. Overall, we obtained a fairly complete picture of how the dynamical response of IF neurons depends on synaptic timescales, including fairly realistic descriptions used in detailed biophysical models.

These results were obtained under certain conditions. First, we assumed no correlation between synaptic inputs. Correlations in the inputs to an IF neuron affect the firing rate (Salinas & Sejnowski, 2000) since they lead to an effective increase or decrease of the variance of the noise, depending on the type of correlation. However, we do not expect qualitative changes in

the neuron dynamical response. Second, we considered synaptic current rather than conductance changes. Qualitative differences between current and conductance inputs were recently pointed out by Tiesinga, Jose, and Sejnowski (2000). As far as the dynamical response is concerned, we do not expect any qualitative difference if conductance-based inputs are considered. Quantitatively, the effective membrane time constant will be reduced by conductance inputs, leading to an increase of the magnitude of the instantaneous component in the response. The two IF neuronal models we investigated show similar qualitative behaviors at high frequencies. The main difference between both models is the presence in the LIF neuron dynamical response, $\hat{n}(\omega)$ of resonant peaks at input frequencies that are multiples of its stationary firing rate. These resonant peaks occur when the background firing rate is high and for low noise, when firing is close to being periodic. They tend to disappear as noise increases. Within the range of firing rate we considered in our simulations (10–50 Hz), the resonant peaks disappear completely at a noise strength σ of order 2 to 5 mV. This corresponds roughly to the orders of magnitude of the noise variance found in measurements in vivo (Destexhe & Paré, 1999). Therefore, the simplest IF neuron could give a good approximation to the dynamics of the leaky IF neuron in conditions similar to in vivo conditions. In the low-noise regime, these resonant peaks give rise to an oscillatory behavior of the instantaneous firing rate in response to step current increase (Marsalek, Koch, & Maunsell, 1997; Burkitt & Clark, 1999; van Rossum, 2001).

Another attempt to include synaptic dynamics into a population density approach has recently been done by Haskell et al. (2001). To get a computationnally efficient description, they reduced the multidimensional partial differential equation describing the dynamics of the population to a one-dimensional one. However, their resulting reduced dynamical equation for the population density does not capture the high-frequency response of the neuron. Indeed, in their model, the mean and the variance of the input are filtered by the synaptic dynamics, but the input variance is still associated with white noise. Consequently, they find that the probability density near threshold is zero for any τ_s. Thus, their approximation can capture the dynamics in response to slowly varying inputs but not the high-fequency behavior.

Our work adds elements to the old debate concerning the dichotomy between spiking and firing-rate neuron models. An important question is whether spiking neuronal models can be reduced to descriptions in terms of firing rates and in which conditions this reduction is possible. In firing-rate neuronal models, the input $I_{in}(t)$ of the neuron usually acts on the firing rate of the neuron $\nu(t)$ through a low-pass filter,

$$\tau \frac{d\nu}{dt} = -\nu(t) + \phi[I_{in}(t)],$$

where ϕ is the neuronal transfer function, but the value of the time constant τ to be used in such a description has been the subject of debate (Treves, 1993;

Abbott & van Vreeswijk, 1993; Gerstner, 1995; Pinto, Brumberg, Simons, & Ermentrout, 1996; Ermentrout, 1998). We showed that in presence of realistic noise, when the synaptic timescale is of the same order as the membrane time constant, the firing rate is able to follow instantaneously current inputs directly injected into the soma. In these conditions, we would essentially have

$$\nu(t) = \phi[I_{in}(t)]. \tag{6.1}$$

In real neurons, inputs come through synapses, and therefore the response to oscillatory inputs is low pass filtered, with an additional factor of $1/(1+i\omega\tau_s)$ in the response in the simplest case of a single synaptic decay time. Thus, instead of the instantaneous response given by equation 6.1, the dynamics will be purely governed by the synaptic decay time,

$$\tau_s \frac{dI_s}{dt} = -I_s(t) + I_{in}(t)$$
$$\nu(t) = \phi[I_s(t)].$$

Such a relationship is valid for small modulations around a finite background firing rate. When the current is such that the firing rate becomes essentially zero, deviations to this behavior are expected (Chance, 2000). We emphasize that the other conditions for which we expect such a reduction to be valid (presence of a finite background firing rate and synaptic time constants of the same order as the membrane time constant) seem to be the typical conditions of a cortical neuron in vivo. For conductance-based synaptic inputs, the bombardment due to spontaneous activity acts to reduce the membrane time constant. This will also contribute to a faster response to external input. Furthermore, when the synaptic timescales are shorter than the membrane timescale, the dynamics of the firing probability can still be reasonably approximated by

$$\nu(t) \sim r_{HF} I_{in}(t) + (1 - r_{HF}) \exp(-t/\tau) \int_{-\infty}^{\tau} \exp(u/\tau) I_{in}(u) \frac{du}{\tau}, \tag{6.2}$$

where r_{HF} is the high-frequency limit of the dynamical response (see equation 5.39) and τ is a time constant typically between τ_s and τ_e for small τ_s. We show examples of this kind of approximation in Figure 10 for the SIF neuron.

The noise model we have studied provides an interpolation between two previously studied noise models: at large τ_s, the rapid changes in response to sharp input transient are similar to what was found in slow noise models (Knight, 1972; Gerstner, 2000), and, at small τ_s, the response is fast only at low noise strengths, as in the fast noise, escape noise model (Gerstner, 2000).

Finally, the methods presented in this article are a prerequisite for an analysis of the dynamics of recurrent neuronal networks in the presence of realistic noise.

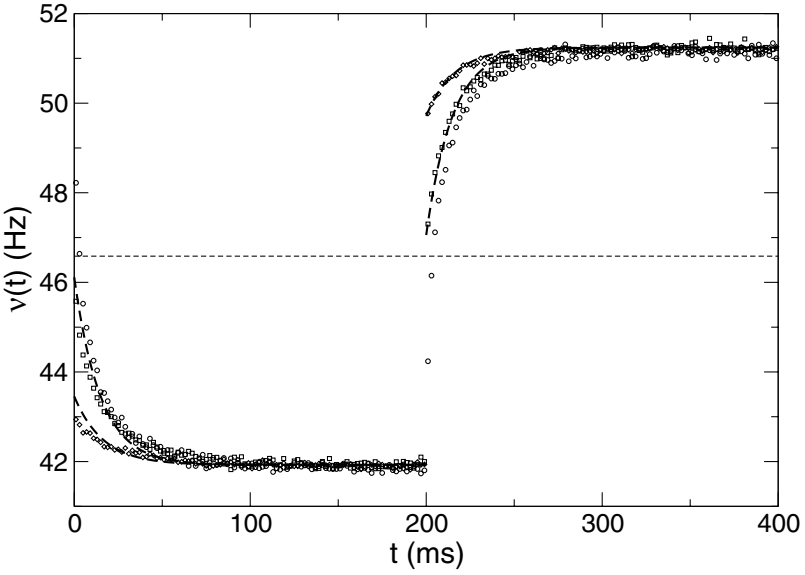

Figure 10: Instantaneous firing rate of the SIF neuron in response to a periodic step input. We show the simulation results for three synaptic times: $\tau_s = 0$ ms (white noise) (○), $\tau_s = 5$ ms (□), and $\tau_s = 20$ ms (◇). In all cases $\tau_e = 20$ ms. Bin size: 1 ms. Note that for finite τ_s, there is an instantaneous jump of the firing rate in response to a discontinuity in the input current. We also plot (dashed lines) an approximation of the response given by equation 6.2 with $T = 14.9$ ms for $\tau_s = 5$ ms and $T = 16.4$ ms for $\tau_s = 20$ ms.

Appendix A: SIF Neuron: Stationary Input

A.1 Firing Probability. The membrane potential obeys

$$\frac{dV}{dt} = I_s(t). \tag{A.1}$$

Each time V reaches the threshold θ, it is immediately reset to V_r. Below the threshold, the membrane potential of the neuron is

$$V(t) = V(0) + \int_0^t I_s(u)\, du.$$

From this equation, it is straightforward to determine the time at which the nth spike is fired. It occurs at the first time t that satisfies

$$\int_0^t I_s(u)\, du = n(\theta - V_r) + V_r - V(0).$$

Thus, the number of spikes the neuron has emitted at time t is given by

$$n(t) = E\left(\sup_{u\le t}\left(\frac{V(0) - V_r + \int_0^u I_s(v)\,dv}{\theta - V_r}\right)\right), \tag{A.2}$$

where $E(x)$ is the integer part of x. Writing I_s as the sum of its mean μ and of its fluctuations $\Delta I_s \equiv I_s - \mu$, we obtain

$$n(t) = E\left(\frac{V(0) - V_r}{\theta - V_r} + \sup_{u\le t}\frac{\mu u + \int_0^u \Delta I_s(v)\,dv}{\theta - V_r}\right). \tag{A.3}$$

The firing probability is computed as

$$\lim_{t\to\infty}\frac{n(t)}{t} = \lim_{t\to\infty}\frac{1}{t}E\left(\sup_{u\le t}\frac{\mu u + \int_0^u \Delta I_s(v)\,dv}{\theta - V_r}\right). \tag{A.4}$$

We show in the next paragraph that the mean of the random variable

$$X = \lim_{t\to\infty}\frac{1}{t}E\left(\sup_{u\le t}\mu u + \int_0^u \Delta I_s(v)\,dv\right) \tag{A.5}$$

is μ. Thus, the mean firing rate is

$$\nu = \lim_{t\to\infty}\frac{n(t)}{t} = \frac{\mu}{\theta - V_r}. \tag{A.6}$$

The firing rate of the SIF neuron is independent of the synaptic time τ_s and the magnitude of the noise σ.

We now compute the mean of the random variable (see equation A.5):

$$X = \lim_{t\to\infty}\frac{1}{t}E\left(\sup_{u\le t}\left(\mu u + \int_0^u \Delta I_s(v)\,dv\right)\right).$$

The quantity inside the parentheses can be bounded above by

$$\sup_{u\le t}\left(\mu u + \int_0^u \Delta I_s(v)\,dv\right) \le \sup_{u\le t}(\mu u) + \sup_{u\le t}\left(\int_0^u \Delta I_s(v)\,dv\right) \tag{A.7}$$

and below by

$$\sup_{u\le t}\left(\mu u + \int_0^u \Delta I_s(v)\,dv\right) \ge \sup_{u\le t}(\mu u) + \inf_{u\le t}\left(\int_0^u \Delta I_s(v)\,dv\right), \tag{A.8}$$

with $\sup_{u\le t}(\mu u) = \mu t$. Since $\Delta I_s(v)$ is a random process symmetric around 0, we need to look only at the upper bound.

First, consider the case where $\Delta I_s(v)$ is a gaussian white noise (instantaneous synaptic current). We can define

$$W_t = \int_0^t \Delta I_s(v)dv = \int_0^t \eta(v)\,dv,$$

which is a Brownian motion with the well-known probability density

$$p(W_t = x, t) = \frac{1}{\sqrt{2\pi\sigma^2 t}} e^{-\frac{x^2}{2\sigma^2 t}}.$$

The running maximum of W_t,

$$S_t = \sup_{u\le t} W_u,$$

obeys (Karatzas & Shreve, 1988)

$$P(S_t = x) = 2P(W_t = x) = 2p(x, t).$$

The mean of S_t is

$$\langle S_t\rangle = \sigma\sqrt{\frac{t}{2\pi}}. \tag{A.9}$$

Hence, it directly follows that $\langle X\rangle = \mu$.

If we now consider the case where we have synaptic currents with relaxation time τ_s,

$$\Delta I_s(v) = \frac{1}{\tau_s}\int_0^v e^{\frac{w-v}{\tau_s}}\,\eta(w)\,dw,$$

we define

$$W'_t = \int_0^v \Delta I_s(v)\,dv$$

and

$$S'_t = \sup_{u\le t} W'_u.$$

ΔI_s is an Ornstein-Uhlenbeck process, and we can compute the probability density of W'_t,

$$p(W'_t = x) = \frac{1}{\sqrt{2\pi\sigma^2\Omega(t)}} e^{-\frac{x^2}{2\sigma^2\Omega(t)}}, \tag{A.10}$$

with $\Omega(t) = t - 2\tau_s \tanh\left(\frac{t}{2\tau_s}\right) + \frac{\tau_s}{2}(1 - e^{-\frac{t}{2\tau_s}}) \tanh\left(\frac{t}{2\tau_s}\right)^2$. Since $\Omega(t) < t$, it follows that the probability density of W'_t will be more peaked than when ΔI_s is white noise. Thus, $\langle S'_t \rangle < \langle S_t \rangle$, and therefore we again find

$$\langle X \rangle = \mu. \tag{A.11}$$

A.2 P.d.f.—White Noise. For simplicity, it is useful to define the adimensional variable and constants:

$$u = \frac{2\tilde{\mu}V}{\tilde{\sigma}^2}, \quad u_\theta = \frac{2\tilde{\mu}\theta}{\tilde{\sigma}^2}, \quad u_r = \frac{2\tilde{\mu}V_r}{\tilde{\sigma}^2}. \tag{A.12}$$

The Fokker-Planck equation (see equation 3.10) written with this variable is

$$\frac{\tau_e}{2}\frac{\partial P_0}{\partial t} = \frac{\partial^2 P_0}{\partial u^2} - \frac{\partial P_0}{\partial u}, \tag{A.13}$$

where

$$\tau_e = \frac{\tilde{\sigma}^2}{\tilde{\mu}^2} \tag{A.14}$$

is a time constant that depends on the signal-to-noise ratio of synaptic inputs. It is the only time constant when synaptic timescales are absent and plays the role of the membrane time constant of the leaky IF neuron, as we will see. Note that if we come back to the original variables, we have in the case $J_i = J$ for all i, $\tau_e = 1/C\nu$ (see equation 3.2).

In this section, we consider the stationary problem $\partial P_0/\partial t = 0$. Thus, we have to solve

$$\frac{\partial^2 P_0}{\partial u^2} = \frac{\partial P_0}{\partial u}, \tag{A.15}$$

and the new boundary conditions are

$$\begin{aligned} P_0(u_\theta) &= 0 \\ \frac{\partial P_0}{\partial u}(u_\theta) &= -\frac{\nu_0\tau_e}{2} \\ P_0(u_{r+}) - P_0(u_{r-}) &= 0 \\ \frac{\partial P_0}{\partial u}(u_{r+}) - \frac{\partial P_0}{\partial u}(u_{r-}) &= -\frac{\nu_0\tau_e}{2}. \end{aligned} \tag{A.16}$$

The solution of equations A.15 and A.16 is

$$P_0(y) = \frac{\nu_0\tau_e}{2}[1 - e^{u-u_\theta} - \Theta(u_r - u)(1 - e^{u-u_r})], \tag{A.17}$$

where Θ is the Heaviside function. The normalization of the probability density P_0 to 1 gives the stationary firing rate given by equation 4.9.

A.3 P.d.f.—Synaptic Noise. In this section, we derive the first-order correction in k to the SIF neuron p.d.f. A summary of the results is given in section 4.2.3. Note that for these calculations, we use $k = \sqrt{\frac{\tau_s}{\tau_e}}$ with τ_e defined in equation A.14.

A.3.1 FP Equation and Boundary Conditions. We can rewrite the FP equation (see equation 4.12) using the rescaled variables u and z defined in equations A.12 and 4.25 as

$$\frac{1}{2}\frac{\partial^2 P}{\partial z^2} + \frac{\partial (zP)}{\partial z} - k\frac{\partial P}{\partial z} - 2kz\frac{\partial P}{\partial u} = 0. \tag{A.18}$$

The boundary conditions with these new variables are

$$zP(u_\theta, z) = \frac{k\tau_e \nu(z)}{2} \tag{A.19}$$

$$z[P(u_{r+}, I_s) - P(u_{r-}, z)] = \frac{k\tau_e \nu(z)}{2} \tag{A.20}$$

$$\lim_{z\to\pm\infty} zP(u, z) = 0 \tag{A.21}$$

$$\lim_{z\to\pm\infty} \frac{\partial P}{\partial z} = 0, \tag{A.22}$$

with the particular condition

$$\nu(z) = P(u_\theta, z) = 0 \quad \text{for all} \quad z < 0. \tag{A.23}$$

We then define

$$P(u, z) = \frac{Q(u, z)}{\sqrt{\pi}} e^{-z^2}. \tag{A.24}$$

Inserting equation A.24 in A.18, we obtain

$$LQ + 2kz\left(Q - \frac{\partial Q}{\partial u}\right) - k\frac{\partial Q}{\partial z} = 0, \tag{A.25}$$

where L is a differential operator defined by

$$L. = \frac{1}{2}\frac{\partial^2 .}{\partial z^2} - z\frac{\partial .}{\partial z}. \tag{A.26}$$

To solve equation A.25 with boundary conditions given by equations A.19 through A.23, we use recent analytical methods described in Hagan et al.

(1989) and Klosek & Hagan (1998) and in the neuronal context in Brunel and Sergi (1998). Q and the firing probability ν are expanded in powers of k,

$$Q = \sum_n k^n Q_n, \quad \nu = \sum_n k^n \nu_n.$$

Q and ν can then be obtained by recurrence:

$$LQ_0 = 0 \tag{A.27}$$

$$LQ_n = \frac{\partial Q_{n-1}}{\partial z} - 2z\left(Q_{n-1} - \frac{\partial Q_{n-1}}{\partial u}\right). \tag{A.28}$$

A.3.2 Solution far from the Boundaries.

Order 0. The solution of equation A.27 is

$$Q_0 = f(u)\int e^{z^2}\,dz + g(u), \tag{A.29}$$

where f and g are functions of u only. Since zP must vanish in both limits $z \to \pm\infty$, we necessarily have $f(u) = 0$. Then at order 0 in k, the problem is equivalent to the white noise case, and we have

$$Q_0(u) = P_0(u), \tag{A.30}$$

where P_0 is given by equation A.17.

Order 1. We obtain from equation A.28

$$LQ_1 = 2z\left(\frac{\partial Q_0}{\partial u} - Q_0\right). \tag{A.31}$$

Q_1 can be written as a sum of the solution of the homogeneous equation $LQ = 0$ and of a particular solution of equation A.31, Q_1^p. The general solution of equation $LQ = 0$ is again

$$Q_1 = f(u)\int e^{z^2}\,dz + g(u). \tag{A.32}$$

Since the right-hand side of equation A.31 is polynomial in z and

$$Lz^n = -nz^n + \frac{n(n-1)}{2}z^{n-2},$$

we look for a particular solution Q_1^p that is polynomial in z:

$$Q_1^p = Q_1^1(u)z + Q_1^0(u). \tag{A.33}$$

Inserting equation A.17 in the right-hand side of equation A.31, we find

$$Q_1^1(u) = \nu_0 \tau_e \Theta(u - u_r). \tag{A.34}$$

Since zP must vanish in both limits $z \to \pm\infty$, we have again $f(u) = 0$ in equation A.32. Thus, we have, absorbing $g(u)$ in $Q_1^0(u)$,

$$Q_1(u, z) = Q_1^1(u)z + Q_1^0(u), \tag{A.35}$$

where Q_1^0 is still to be determined.

Order 2. Using the same method, we find

$$Q_2(u, z) = Q_2^0(u) + 2\left(1 - \frac{\partial}{\partial u}\right) Q_1^0(u)z + \Theta(u - u_r)\nu_0 \tau_e z^2. \tag{A.36}$$

Order 3. At this order, we find that to satisfy the boundary condition A.21, we need Q_1^0 to obey the condition

$$\frac{\partial^2 Q_1^0}{\partial u^2} = \frac{\partial Q_1^0}{\partial u}. \tag{A.37}$$

To get $Q_1^0(u)$, we still need to specify the boundary conditions it satisfies. These will be provided by the boundary layer solutions.

A.3.3 Threshold Layer Solution. The second step is to determine the solution of equation A.31 near the threshold u_θ. Since the area close to the threshold where the boundary solution departs from the outer solution is expected to be of width k (Hagan et al., 1989), we define

$$x = \frac{u_\theta - u}{k}, \tag{A.38}$$

and we look for a solution $Q^T(x, z)$ that matches the boundary condition at $x = 0$ and the outer solution for large x. We also expand this function in k, and the equations for the first orders in k, Q_0^T and Q_1^T, are

$$LQ_0^T + 2z\frac{\partial Q_0^T}{\partial x} = 0 \tag{A.39}$$

$$LQ_1^T + 2z\frac{\partial Q_1^T}{\partial x} = \left(\frac{\partial Q_0^T}{\partial z} - 2zQ_0^T\right). \tag{A.40}$$

According to equation 4.18, we know that $Q^T(x = 0, z) = 0$ for any $z < 0$. The $x \to \infty$ limits of $Q^T(x, z)$ are given by the boundary conditions of the

outer solution Q_0 in u_θ. Using equations 4.8 and A.35, we find that

$$\lim_{x\to+\infty} Q_0^T(x) = Q_0(u_\theta) = 0 \tag{A.41}$$

$$\begin{aligned}\lim_{x\to+\infty} Q_1^T(x,z) &= Q_1(u_\theta,z) - x\frac{\partial Q_0}{\partial u}(u_\theta)\\ &= Q_1^0(u_\theta) + \frac{\nu_0\tau_e}{2}(x+2z).\end{aligned} \tag{A.42}$$

The solution of equations A.39 through A.42 is (Hagan et al., 1989)

$$Q_0^T(x,z) = 0 \tag{A.43}$$

$$Q_1^T(x,z) = \frac{\nu_0\tau_e}{2}\left(\alpha + x + 2z + \sum_{n=1}^{+\infty}\beta_n v_n^+(\sqrt{2}z)e^{-\sqrt{\frac{n}{2}}x}\right), \tag{A.44}$$

with

$$\alpha = \sqrt{2}\left|\zeta\left(\frac{1}{2}\right)\right| \tag{A.45}$$

$$\beta_n = -\frac{N(\sqrt{n})}{\sqrt{2}n!\sqrt{n}} \tag{A.46}$$

$$v_n^+(z) = e^{\frac{z^2}{4}}e^{-\frac{(z+2\sqrt{n})^2}{4}}He_n(z+2\sqrt{n}), \tag{A.47}$$

where ζ is the Riemann zeta function, He_n is the nth Hermite polynomial (Abramowitz & Stegun, 1970), and

$$N(s) = \prod_{k=1}^{\infty}\left(1+\frac{s}{\sqrt{k}}\right)e^{-2s(\sqrt{k}-\sqrt{k-1})}\left(\frac{k+1}{k}\right)^{\frac{s^2}{2}}. \tag{A.48}$$

Note that α and β_ns differ from those used in Hagan et al. (1989) by a factor $\sqrt{2}$.

A.3.4 Reset-Layer Solution. To complete the description of the first-order correction of the p.d.f., we have to look at the boundary solution near $u = u_r$. As in equation A.38, we define

$$v = \frac{u_r - u}{k}, \tag{A.49}$$

and we look for solutions $Q_1^{R+}(v,z)$ and $Q_1^{R-}(v,z)$ matching the boundary condition at $v = 0$ and the outer solution for large v, respectively, for $v < 0$ and $v > 0$. The equation for Q_1^R is

$$LQ_1^R - 2z\frac{\partial Q_1^R}{\partial v} = \left(\frac{\partial Q_0^R}{\partial z} - 2zQ_0^R\right). \tag{A.50}$$

Using equations A.17 and A.35, we find

$$\lim_{v\to\pm\infty} Q_0^{R\pm}(v) = Q_0^{\pm}(u_r) = 0 \tag{A.51}$$

$$\lim_{v\to-\infty} Q_1^{R+}(v,z) = Q_1^{+}(u_r,z) - v\frac{\partial Q_0^{+}}{\partial u}(u_r) = Q_1^{0+}(u_r) + \frac{\nu_0\tau_e}{2}(2z + e^{u_r-u_\theta}v) \tag{A.52}$$

$$\lim_{v\to+\infty} Q_1^{R-}(v,z) = Q_1^{-}(u_r,z) - v\frac{\partial Q_0^{-}}{\partial u}(u_r) = Q_1^{0-}(u_r) + \frac{\nu_0\tau_e}{2}(e^{u_r-u_\theta} - 1)v. \tag{A.53}$$

According to equations 4.19 and 4.20, we know that $Q_1^{R+}(0,z) - Q_1^{R-}(0,z) = Q_1^{T}(0,z)$. We find

$$Q_0^{R\pm}(v,z) = 0 \tag{A.54}$$

$$Q_1^{R+}(v,z) = Q_1^{0+}(u_r) + \frac{\nu_0\tau_e}{2}(e^{y_r-y_\theta}v + 2z) \tag{A.55}$$

$$Q_1^{R-}(v,z) = Q_1^{0-}(u_r) + \frac{\nu_0\tau_e}{2} \times \left((e^{u_r-u_\theta} - 1)v - \sum_{n=1}^{+\infty}\beta_n v_n^{+}(\sqrt{2}z)e^{-\sqrt{\frac{\pi}{2}}v}\right). \tag{A.56}$$

According to equation A.37, we have

$$Q_1^0(u) = A_1^0 e^u + B_1. \tag{A.57}$$

Then, knowing the boundary conditions (given by equation A.42) and that the sum of Q_1^0 over y should be 0 since it is a correction to a probability density, we find

$$Q_1^{0+}(u_r) = \frac{\nu_0\tau_e}{2}\alpha e^{u_r-u_\theta} \tag{A.58}$$

$$Q_1^{0-}(u_r) = \frac{\nu_0\tau_e}{2}\alpha(e^{u_r-u_\theta} - 1), \tag{A.59}$$

where α has been defined in equation A.45.

Appendix B: SIF Neuron: Oscillatory Input

B.1 White Noise. We can rewrite the FP equation using the variable u (see equation A.12) as

$$\frac{\tau_e}{2}\frac{\partial \mathcal{P}}{\partial t} = \frac{\partial^2 \mathcal{P}}{\partial u^2} - (1 + \epsilon e^{i\omega t})\frac{\partial \mathcal{P}}{\partial u}, \tag{B.1}$$

and the boundary conditions are now

$$\mathcal{P}(u_\theta, t) = 0 \tag{B.2}$$

$$\frac{\partial \mathcal{P}}{\partial u}(u_\theta, t) = -\frac{\nu(t)\tau_e}{2} \tag{B.3}$$

$$\mathcal{P}(u_{r+}, t) - \mathcal{P}(u_{r-}, t) = 0 \tag{B.4}$$

$$\frac{\partial \mathcal{P}}{\partial u}(u_{r+}, t)) - \frac{\partial \mathcal{P}}{\partial u}(u_{r-}, t) = -\frac{\nu(t)\tau_e}{2}. \tag{B.5}$$

Our strategy is to solve equation B.1 with its associated boundary conditions using an expansion in the small parameter ϵ. Thus, we write

$$\nu(t) = \nu_0[1 + \epsilon e^{i\omega t}\hat{n}(\omega) + O(\epsilon^2)] \tag{B.6}$$

$$\mathcal{P}(u, t) = P(u) + \epsilon e^{i\omega t}\hat{P}(u, \omega) + O(\epsilon^2), \tag{B.7}$$

where $\hat{n}(\omega)$ and $\hat{P}(u, \omega)$ are complex quantities describing the oscillatory component at the frequency input ω of the instantaneous firing rate and the voltage probability density.

The zeroth order gives the stationary response ν_0 and $P(u)$ given by equations A.6 and A.17.

At the first order in ϵ, we have

$$\frac{i\tau_e\omega}{2}\hat{P}(u, \omega) = \frac{\partial^2 \hat{P}}{\partial u^2} - \frac{\partial \hat{P}}{\partial u} - \frac{dP}{du}, \tag{B.8}$$

with the boundary conditions

$$\begin{aligned}
\hat{P}(u_\theta, \omega) &= 0 \\
\frac{\partial \hat{P}}{du}(u_\theta, \omega) &= -\frac{\hat{n}(\omega)\nu_0\tau_e}{2} \\
\hat{P}(u_{r+}, \omega) - \hat{P}(u_{r-}, \omega) &= 0 \\
\frac{\partial \hat{P}}{du}(u_{r+}, \omega)) - \frac{\partial \hat{P}}{du}(u_{r-}, \omega) &= -\frac{\hat{n}(\omega)\nu_0\tau_e}{2}.
\end{aligned} \tag{B.9}$$

Solutions of equation B.8 are linear combinations of two exponentials $\exp(r_\pm(\omega))$ where

$$r_\pm(\omega) = \frac{1 \pm \sqrt{1 + 2i\tau_e\omega}}{2}, \tag{B.10}$$

plus the particular solution

$$\hat{P}^p = -\frac{2}{i\tau_e\omega}\frac{dP}{du}.$$

The coefficients of the exponentials are obtained using the boundary conditions, equation B.9. We obtain

$$\hat{P}(u,\omega) = \frac{\nu_0}{i\omega}[e^{u-u_\theta} - e^{r_+(\omega)(u-u_\theta)} - \Theta(u_r - u)(e^{u-u_r} - e^{r_+(\omega)(u-u_r)})] \tag{B.11}$$

and

$$\hat{n}(\omega) = \frac{\sqrt{1 + 2i\tau_e\omega} - 1}{i\tau_e\omega}. \tag{B.12}$$

B.2 Synaptic Noise. Note that for these calculations, we use $k = \sqrt{\frac{\tau_s}{\tau_e}}$ with τ_e defined in equation A.14.

B.2.1 FP Equation and Boundary Conditions. The FP equation associated with see equations 3.5 and 3.6, using again the variables u, equation A.12, and z, equation 5.18, is

$$k^2\tau_e\frac{\partial\mathcal{P}}{\partial t} = \frac{1}{2}\frac{\partial^2\mathcal{P}}{\partial z^2} + \frac{\partial(z\mathcal{P})}{\partial z} - k\frac{\partial\mathcal{P}}{\partial z} - \epsilon e^{i\omega t}k(1 + k^2 i\omega\tau_e)\frac{\partial\mathcal{P}}{\partial z} - 2kz\frac{\partial\mathcal{P}}{\partial u}. \tag{B.13}$$

As in equation 4.17, the instantaneous firing rate is given by the probability flux in the z direction through u_θ integrated over z,

$$\nu(t) = \int_{-\infty}^{+\infty} J_u(u_\theta, z, t)\, dz, \tag{B.14}$$

with J_u defined by

$$\frac{\partial\mathcal{P}}{\partial t} + \frac{\partial J_u}{\partial u} + \frac{\partial J_z}{\partial z} = 0 \tag{B.15}$$

and so

$$J_u = \frac{2z}{k\tau_e}\mathcal{P}. \tag{B.16}$$

Note that due to the factor $\frac{1}{k}$ in the expression of J_u, we have to expand $\mathcal{P}$ to the second order in k to obtain the first-order correction to the instantaneous firing rate.

The particular boundary condition is again (compare with equation 4.18)

$$J_u(u_\theta, z, t) = 0, \quad \text{for all} \quad z < 0. \tag{B.17}$$

The other boundary conditions at equal z or u are the same as in the case without synaptic relaxation and hold at any time t.

We look at the linear response to the oscillation and have at the first order in ϵ,

$$k^2 i\omega\tau_e \hat{P} = \frac{1}{2}\frac{\partial^2 \hat{P}}{\partial z^2} + \frac{\partial(z\hat{P})}{\partial z} - k\frac{\partial \hat{P}}{\partial z} - k(1 + k^2 i\omega\tau_e)\frac{\partial P}{\partial z} - 2kz\frac{\partial \hat{P}}{\partial u}. \tag{B.18}$$

We again solve the equation by expanding the density probability in k. We note

$$P = P_0 + kP_1 + k^2 P_2 + \cdots \tag{B.19}$$

$$\hat{P} = \hat{P}_0 + k\hat{P}_1 + k^2\hat{P}_2 + \cdots \tag{B.20}$$

Analytical solutions can be found in two opposite limits: at low frequencies $\omega \sim \frac{1}{\tau_e}$ and at high frequencies $\omega \gg \frac{1}{\tau_s}$. To connect these two limits, we resort to numerical solutions.

B.2.2 Outer Solution. We first define $\mathcal{Q}$ by

$$\mathcal{P}(u, z, t) = \mathcal{Q}(u, z, t)\frac{e^{-z^2}}{\sqrt{\pi}}. \tag{B.21}$$

Then we expand $\mathcal{Q}$ in ϵ and k,

$$\mathcal{Q} = Q + \epsilon e^{i\omega t}\hat{Q} + O(\epsilon^2) = \sum_n k^n (Q_n + \epsilon e^{i\omega t}\hat{Q}_n) + O(\epsilon^2). \tag{B.22}$$

By inserting equation B.21 into equation 5.26, we find the equation for $\hat{Q}$:

$$\begin{aligned} L\hat{Q} = {} & k\frac{\partial \hat{Q}}{\partial z} + 2kz\left(\frac{\partial \hat{Q}}{\partial u} - \hat{Q}\right) + k^2 i\omega\tau_e\hat{Q} \\ & + k(1 + k^2 i\omega\tau_e)\left(\frac{\partial Q}{\partial z} - 2zQ\right). \end{aligned} \tag{B.23}$$

The operator L has been defined in equation A.26, and the first orders of Q are given in section 4.2.3.

Order 0. At the zeroth order in k, we have

$$L\hat{Q}_0 = 0. \tag{B.24}$$

Since $\hat{Q}$ must vanish for $z \to \pm\infty$, we necessarily have

$$\hat{Q}_0(u, z, \omega) = \hat{P}(u, \omega), \tag{B.25}$$

where $\hat{P}(u, \omega)$ is given by equation B.11.

Order 1. $\hat{Q}_1$ is given by

$$L\hat{Q}_1 = 2z\left(\frac{\partial \hat{Q}_0}{\partial u} - \hat{Q}_0\right) - 2zQ_0. \tag{B.26}$$

By noting

$$\hat{Q}_1(u, z, \omega) = \hat{Q}_1^0(u, \omega) + z\hat{Q}_1^1(u, \omega) \tag{B.27}$$

and inserting it in equation B.26, we find

$$\hat{Q}_1^1 = 2\left(\hat{Q}_0 - \frac{\partial \hat{Q}_0}{\partial u}\right) + 2Q_0. \tag{B.28}$$

The expansion of $\hat{Q}$ until the third order leads to an equation for $\hat{Q}_1^0$,

$$\frac{\partial^2 \hat{Q}_1^0}{\partial y^2} - \frac{\partial \hat{Q}_1^0}{\partial u} = \frac{i\omega\tau_e}{2}\hat{Q}_1^0 + \frac{\partial Q_1^0}{\partial u}. \tag{B.29}$$

We will solve it later after we have specified the boundary conditions for $\hat{Q}_1^0$.

Order 2. Then $\hat{Q}_2$ is given by

$$L\hat{Q}_2 = \frac{\partial \hat{Q}_1}{\partial z} + 2z\left(\frac{\partial \hat{Q}_1}{\partial u} - \hat{Q}_1\right) + \frac{\partial Q_1}{\partial z} - 2zQ_1 + i\omega\tau_e\hat{Q}_0. \tag{B.30}$$

Again, we look for a solution polynomial in z, and we note

$$\hat{Q}_2(u, z, \omega) = \hat{Q}_2^0(u, \omega) + z\hat{Q}_2^1(u, \omega) + \frac{z^2}{2}\hat{Q}_2^2(u, \omega). \tag{B.31}$$

By inserting it into equation B.30, we find for the terms proportional to z^2 and z,

$$\hat{Q}_2^2(u,\omega) = 2\hat{Q}_1^1 - 2\frac{\partial \hat{Q}_1^1}{\partial u} + 2Q_1^1 \tag{B.32}$$

$$\hat{Q}_2^1(u,\omega) = 2\hat{Q}_1^0 - 2\frac{\partial \hat{Q}_1^0}{\partial u} + 2Q_1^0. \tag{B.33}$$

Since $L.1 = 0$, the resting terms should vanish, and we have the equation

$$\frac{\partial^2 \hat{Q}_0}{\partial u^2} - \frac{\partial \hat{Q}_0}{\partial u} = \frac{i\omega\tau_e}{2}\hat{Q}_0 + \frac{\partial Q_0}{\partial u}. \tag{B.34}$$

Note that a comparison of the above with equation B.8 confirms the result, equation B.25. We could obtain a similar equation for $\hat{Q}_2^0$ by looking at the fourth order in k, but we do not need it since $\hat{Q}_2^0$ will not intervene in the calculation of the firing rate.

B.2.3 Threshold Solution. Following the method developed in section 4.2.2, we now look at the threshold solution noted $\hat{Q}^T$. We define

$$x = \frac{u_\theta - u}{k}. \tag{B.35}$$

Then equation B.23 becomes

$$\begin{aligned} L\hat{Q}^T + 2z\frac{\partial \hat{Q}^T}{\partial x} = k\frac{\partial \hat{Q}^T}{\partial z} - 2kz\hat{Q}^T + k^2 i\omega\tau_e\hat{Q}^T \\ + k(1 + k^2 i\omega\tau_e)\left(\frac{\partial Q^T}{\partial z} - 2zQ^T\right). \end{aligned} \tag{B.36}$$

We first solve this equation at the order 0 and 1 in k. The equations for $\hat{Q}_0^T$ and $\hat{Q}_1^T$ are

$$L\hat{Q}_0^T + 2z\frac{\partial \hat{Q}_0^T}{\partial x} = 0 \tag{B.37}$$

$$L\hat{Q}_1^T + 2z\frac{\partial \hat{Q}_1^T}{\partial x} = \frac{\partial \hat{Q}_0^T}{\partial z} - 2z\hat{Q}_0^T - 2zQ_0^T. \tag{B.38}$$

Moreover, according to equations B.25, 5.12, and B.27, we have

$$\lim_{x\to\infty} \hat{Q}_0^T = \hat{Q}_0(u_\theta) = 0 \tag{B.39}$$

$$\lim_{x\to\infty} \hat{Q}_1^T = \hat{Q}_1(u_\theta) - x\frac{\partial \hat{Q}_0}{\partial u}(u_\theta) = \hat{Q}_1^0(u_\theta) + \frac{\nu_0\tau_e\hat{n}(\omega)}{2}(x + 2z). \tag{B.40}$$

Thanks to equation 5.24, we know that $\hat{Q}(u,z,\omega) = 0$, for all $z < 0$.

According to Hagan et al. (1989), the solutions are

$$\hat{Q}_0^T = 0 \tag{B.41}$$

$$\hat{Q}_1^T = \frac{\nu_0 \tau_e \hat{n}(\omega)}{2} \left(\alpha + x + 2z + \sum_n \beta_n v_n^+(\sqrt{2}z) e^{-\sqrt{\frac{n}{2}}x} \right), \tag{B.42}$$

where α, β_n, and v_n^+ have been defined in section A.3.3.

We now look at the second order in k. We have

$$L\hat{Q}_2^T + 2z\frac{\partial \hat{Q}_2^T}{\partial x} = \frac{\partial \hat{Q}_1^T}{\partial z} - 2z\hat{Q}_1^T + \frac{\partial Q_1^T}{\partial z} - 2zQ_1^T. \tag{B.43}$$

Since $\{1, \sqrt{2}z, v_n^{\pm}(\sqrt{2}z)\}$ form a complete set of eigenfunctions of L (Hagan et al., 1989), we seek a solution of the form

$$\hat{Q}_2^T(x,z) = \alpha\left(\frac{x}{\sqrt{2}}\right) + \tilde{\alpha}\left(\frac{x}{\sqrt{2}}\right)\sqrt{2}z + \sum_{n,\epsilon=\pm} \alpha_{2_n}^{\epsilon}\left(\frac{x}{\sqrt{2}}\right) v_n^{\epsilon}(\sqrt{2}z). \tag{B.44}$$

By inserting it into equation B.43 and projecting it on the various orthogonal functions, we find

$$\begin{aligned}
\frac{d\alpha}{dx}(x) - \tilde{\alpha}(x) &= \frac{\nu_0 \tau_e}{\sqrt{2}}(1 + \hat{n}(\omega)) \\
&\quad \times \left(\sum_n \beta_n \langle z, v_n^{+'}(z) \rangle e^{-\sqrt{n}x} - (\alpha + x) \right) \\
\frac{d\tilde{\alpha}}{dx}(x) &= 0 \qquad \text{(B.45)} \\
\frac{d\alpha_{2n}^{\epsilon}}{dx}(x) + \epsilon\sqrt{n}\alpha_{2n}^{\epsilon}(x) &= \frac{\nu_0 \tau_e}{\sqrt{2}}(1 + \hat{n}(\omega)) \ldots \\
&\quad \times \left(\left\langle \frac{1}{z}, v_n^{\epsilon}(z) \right\rangle \right. \\
&\quad \left. + \sum_n \beta_n \left\langle v_n^{\epsilon}(z), \frac{v_n^{+'}(z)}{z} - v_n^{+}(z) \right\rangle e^{-\sqrt{n}x} \right),
\end{aligned}$$

where $\langle ., . \rangle$ is an inner product defined by

$$\langle u(z), v(z) \rangle = \frac{1}{\sqrt{\pi}} \int_{-\infty}^{+\infty} e^{-z^2} u(z) v(z)\, dz. \tag{B.46}$$

To achieve the derivation of the first order of the firing-rate expansion in this regime, we need to know only the coefficient $\tilde{\alpha}(x)$. According to

equation B.45, we know it is a constant. It can be determined by looking at the limit $x \to \infty$ where the threshold solution needs to match the outer solution,

$$\lim_{x\to\infty} \tilde{\alpha}(x) = \hat{Q}_2^1(u_\theta). \tag{B.47}$$

According to equation B.33, we need to compute $\hat{Q}_1^0$, which can be done by solving equation B.29. The boundary conditions for $\hat{Q}_1^0$ are given by equation B.42 and by using equations 4.19 through 4.21. We also need to use the fact that the sum of $\hat{Q}_1^0$ over y is zero. Finally, we find

$$\begin{aligned}\hat{Q}_1^0(u,\omega) = \frac{\sqrt{2}\nu_0\alpha}{i\omega}[&r_+(\omega)e^{r_+(\omega)(u-u_\theta)} - e^{u-u_\theta}\ldots \\ &- \Theta(u_r-u)(r_+(\omega)e^{r_+(\omega)(u-u_r)} - e^{u-u_r})],\end{aligned} \tag{B.48}$$

where $r_+(\omega)$ has been defined in equation B.10.

Introducing this last equation in equations B.33 and B.47, we find

$$\tilde{\alpha}(x) = 0. \tag{B.49}$$

We can now compute the first order of the correction,

$$\hat{n}_1(t) = \int_{-\infty}^{+\infty} \frac{2z}{\tau_e}\hat{P}_2(u,z,t)\,dz = \frac{2}{\tau_e}\langle z, \hat{Q}_2^T(0,z)\rangle e^{i\omega t} = 0. \tag{B.50}$$

The last result rises because we have $\langle z, v_n^\epsilon(z)\rangle = 0$ for all n and ϵ.

Appendix C: LIF Neuron

C.1 Stationary Input—Synaptic Noise. We follow the same method as for the SIF case (see section A.3)

C.1.1 Outer Solution. We note

$$y = \frac{V-\mu}{\sigma}.$$

The probability density $P(y,z)$ is

$$P(y,z) = \frac{e^{-z^2}}{\sqrt{\pi}}[Q_0(y) + \sqrt{\tau_s}\tau_m(Q_1^0(y) + zQ_1^1(y))],$$

where Q_0 is given by equation 4.10,

$$\begin{aligned}Q_1^0(y) = \alpha\nu_0\tau_m\sqrt{2}[&-(\Psi(y_\theta) - \Psi(y_r))Q_0(y) \\ &+ e^{-y^2}(e^{y_\theta^2} - e^{y_r^2}\Theta(y_r - y))]\end{aligned} \tag{C.1}$$

and Q_1^1 by

$$Q_1^1(y) = -2y_\theta Q_0(y) - \frac{\partial Q_0}{\partial y}.$$

C.1.2 Boundary-Layer Solutions. The threshold and reset solutions are identical to the SIF, equations 4.32.

C.2 Oscillatory Input—White Noise. The stochastic equation we consider is now

$$\tau_m \frac{dV}{dt} = -V(t) + \mu(1 + \epsilon e^{i\omega t}) + \sigma\sqrt{\tau_m}\eta(t), \tag{C.2}$$

where $\eta(t)$ is a gaussian white noise defined as in equation 3.1. The equivalent Fokker-Planck equation is

$$\tau_m \frac{\partial \mathcal{P}_0}{\partial t} = \frac{\sigma^2\tau_m}{2}\frac{\partial^2 \mathcal{P}_0}{\partial V^2} + \frac{\partial}{\partial V}[V - \mu(1 + \epsilon e^{i\omega t})]\mathcal{P}_\prime. \tag{C.3}$$

The boundary conditions are again identical to the SIF case. We expand both p.d.f. and firing rate in the modulation amplitude ϵ. The amplitude of the modulation in the probability $\hat{P}_0(V, \omega)$ is given by the first order in that expansion,

$$\frac{\sigma^2\tau_m}{2}\frac{\partial^2 \hat{P}_0}{\partial V^2} + \frac{\partial}{\partial V}[V - \mu]\hat{P}_0 - i\omega\tau_m\hat{P}_0 - \mu\frac{\partial P_0}{\partial V} = 0. \tag{C.4}$$

The main difficulty compared to the SIF case is that the general solution to equation C.4 that gives $\hat{P}$ is no longer a linear combination of exponentials (see equations B.8 and B.10) but rather a linear combination of confluent hypergeometric functions (Brunel & Hakim, 1999). Note that these solutions can also be expressed in terms of parabolic cylinder functions (Melnikov, 1993; Lindner & Schimansky-Geier, 2001). However, these functions share the asymptotic properties of the exponentials found in the SIF case; in the high-frequency limit, they behave as $\exp(\sqrt{2i\omega\tau_m}(V-\mu)/\sigma)$. The dynamical linear response of the neuron is

$$\hat{n}(\omega) = \frac{\mu}{\sigma(1 + i\omega\tau_m)}\frac{\frac{\partial U}{\partial y}(y_\theta, \omega) - \frac{\partial U}{\partial y}(y_r, \omega)}{U(y_\theta, \omega) - U(y_r, \omega)}, \tag{C.5}$$

where $y_\theta = \frac{\theta-\mu}{\sigma}$, $y_r = \frac{V_r-\mu}{\sigma}$ and U is given in terms of combinations of hypergeometric functions (Abramowitz & Stegun, 1970),

$$U(y, \omega) = \frac{e^{y^2}}{\Gamma\left(\frac{1+i\omega\tau_m}{2}\right)} M\left(\frac{1 - i\omega\tau_m}{2}, \frac{1}{2}, -y^2\right)$$

$$+\frac{2ye^{y^2}}{\Gamma\left(\frac{i\omega\tau_m}{2}\right)}M\left(1-\frac{i\omega\tau_m}{2},\frac{3}{2},-y^2\right). \tag{C.6}$$

In the high-frequency limit,

$$\hat{n}(\omega)\sim\sqrt{\frac{2}{i\omega\tau_e}}. \tag{C.7}$$

Acknowledgments

We thank Larry Abbott, Frances Chance, Vincent Hakim, David Hansel and Carl van Vreeswijk for useful discussions related to the topics discussed in this article and for their comments on the manuscript.

References

Abbott, L. F., & van Vreeswijk, C. (1993). Asynchronous states in a network of pulse-coupled oscillators. *Phys. Rev. E, 48*, 1483–1490.

Abramowitz, M., & Stegun, I. A. (1970). *Tables of mathematical functions*. New York: Dover.

Amit, D. J., & Tsodyks, M. V. (1991). Quantitative study of attractor neural network retrieving at low spike rates I: Substrate—spikes, rates and neuronal gain. *Network, 2*, 259–274.

Angulo, M. C., Rossier, J., & Audinat, E. (1999). Postsynaptic glutamate receptors and integrative properties of fast-spiking interneurons in the rat neocortex. *J. Neurophysiol., 82*, 1295–1302.

Brunel, N. (2000). Dynamics of sparsely connected networks of excitatory and inhibitory spiking neurons. *J. Comput. Neurosci., 8*, 183–208.

Brunel, N., Chance, F., Fourcaud, N., & Abbott, L. (2001). Effects of synaptic noise and filtering on the frequency response of spiking neurons. *Phys. Rev. Lett., 86*, 2186–2189.

Brunel, N., & Hakim, V. (1999). Fast global oscillations in networks of integrate-and-fire neurons with low firing rates. *Neural Computation, 11*, 1621–1671.

Brunel, N., & Sergi, S. (1998). Firing frequency of integrate-and-fire neurons with finite synaptic time constants. *J. Theor. Biol., 195*, 87–95.

Burkitt, A. N., & Clark, G. M. (1999). Analysis of integrate-and-fire neurons: Synchronization of synaptic input and spike output. *Neural Computation, 11*, 871–901.

Burns, B. D., & Webb, A. C. (1976). The spontaneous activity of neurons in the cat's cerebral cortex. *Proc. R. Soc. Lond. B, 194*, 211–223.

Chance, F. (2000). *Modeling cortical dynamics and the responses of neurons in the primary visual cortex*. Unpublished doctoral dissertation, Brandeis University.

Destexhe, A., Mainen, Z. F., & Sejnowski, T. J. (1998). Kinetic models of synaptic transmission. In C. Koch & I. Segev (Eds.), *Methods in neuronal modeling* (2nd ed., pp. 1–25). Cambridge, MA: MIT Press.

Destexhe, A., & Paré, D. (1999). Impact of network activity on the integrative properties of neocortical pyramidal neurons in vivo. *J. Neurophysiol., 81*, 1531–1547.

Ermentrout, G. B. (1998). Neural networks as spatio-temporal pattern-forming systems. *Rep. Prog. Phys., 61*, 353–430.

Fusi, S., & Mattia, M. (1999). Collective behavior of networks with linear (VLSI) integrate and fire neurons. *Neural Computation, 11*, 633–652.

Gerstner, W. (1995). Time structure of the activity in neural network models. *Phys. Rev. E, 51*, 738–758.

Gerstner, W. (2000). Population dynamics of spiking neurons: Fast transients, asynchronous states, and locking. *Neural Computation, 12*, 43–89.

Gupta, A., Wang, Y., & Markram, H. (2000). Organizing principles for a diversity of GABAergic interneurons and synapses in the neocortex. *Science, 287*, 273–278.

Hagan, P. S., Doering, C. R., & Levermore, C. D. (1989). Mean exit times for particles driven by weakly colored noise. *SIAM J. Appl. Math., 49*, 1480–1513.

Haskell, E., Nykamp, D., & Tranchina, D. (2001). Population density methods for large-scale modelling of neuronal networks with realistic synaptic kinetics: Cutting the dimension down to size. *Network: Comput. Neural Syst., 12*, 141–174.

Hestrin, S., Sah, P., & Nicoll, R. (1990). Mechanisms generating the time course of dual component excitatory synaptic currents recorded in hippocampal slices. *Neuron, 5*, 247–253.

Karatzas, I., & Shreve, S. (1988). *Brownian motion and stochastic calculus*. Berlin: Springer-Verlag.

Klosek, M. M., & Hagan, P. S. (1998). Colored noise and a characteristic level crossing problem. *J. Math. Phys., 39*, 931–953.

Knight, B. W. (1972). Dynamics of encoding in a population of neurons. *J. Gen. Physiol., 59*, 734–766.

Knight, B. W., Omurtag, A., & Sirovich, L. (2000). The approach of a neuron population firing rate to a new equilibrium: An exact theoretical result. *Neural Computation, 12*, 1045–1055.

Lapicque, L. (1907). Recherches quantitatives sur l'excitation électrique des nerfs traitée comme une polarisation. *J. Physiol. (Paris), 9*, 620–635.

Lindner, B., & Schimansky-Geier, L. (2001). Transmission of noise coded versus additive signals through a neuronal ensemble. *Phys. Rev. Lett., 86*, 2934–2937.

Marsalek, P. R., Koch, C., & Maunsell, J. (1997). On the relationship between synaptic input and spike output jitter in individual neurons. *Proc. Natl. Acad. Sci., 94*, 735–740.

McCormick, D., Connors, B., Lighthall, J., & Prince, D. (1985). Comparative electrophysiology of pyramidal and sparsely spiny stellate neurons in the neocortex. *J. Neurophysiol., 54*, 782–806.

Melnikov, V. I. (1993). Schmitt trigger: A solvable model of stochastic resonance. *Phys. Rev. E, 48*, 2481–2489.

Nykamp, D. Q., & Tranchina, D. (2000). A population density approach that facilitates large-scale modeling of neural networks: Analysis and an application to orientation tuning. *J. Comp. Neurosci., 8*, 19–30.

Nykamp, D. Q., & Tranchina, D. (2001). A population density approach that facilitates large-scale modeling of neural networks: Extension to slow inhibitory synapses. *Neural Computation, 13*, 511–546.

Pinto, D. J., Brumberg, J. C., Simons, D. J., & Ermentrout, G. B. (1996). A quantitative population model of whisker barrels: Re-examining the Wilson-Cowan equations. *J. Comput. Neurosci., 3*, 247–264.

Risken, H. (1984). *The Fokker-Planck equation: Methods of solution and applications*. Berlin: Springer-Verlag.

Sah, P., Hestrin, S., & Nicoll, R. A. (1990). Properties of excitatory postsynaptic currents recorded in vitro from rat hippocampal interneurones. *J. Physiol., 430*, 605–616.

Salin, P. A., & Prince, D. A. (1996). Spontaneous $GABA_A$ receptor mediated inhibitory currents in adult rat somatosensory cortex. *J. Neurophysiol., 75*, 1573–1588.

Salinas, E., & Sejnowski, T. J. (2000). Impact of correlated synaptic input on output firing rate and variability in simple neuronal models. *Journal of Neuroscience, 20*, 6193–6209.

Softky, W. R., & Koch, C. (1993). The highly irregular firing of cortical cells is inconsistent with temporal integration of random EPSPs. *J. Neurosci., 13*, 334–350.

Spruston, N., Jonas, P., & Sakmann, B. (1995). Dendritic glutamate receptor channel in rat hippocampal CA3 and CA1 pyramidal neurons. *J. Physiol., 482*, 325–352.

Tiesinga, P. H. E., Jose, J. V., & Sejnowski, T. J. (2000). Comparison of current-driven and conductance-driven neocortical model neurons with Hodgkin-Huxley voltage-gated channels. *Phys. Rev. E, 62*, 8413–8419.

Treves, A. (1993). Mean-field analysis of neuronal spike dynamics. *Network, 4*, 259–284.

Tuckwell, H. C. (1988). *Introduction to theoretical neurobiology*. Cambridge: Cambridge University Press.

van Rossum, M. C. W. (2001). The transient precision of integrate-and-fire neurons: Effect of background activity and noise. *J. Comput. Neurosci., 10*, 303–311.

Wang, X.-J. (1999). Synaptic basis of cortical persistent activity: The importance of NMDA receptors to working memory. *J. Neurosci., 19*, 9587–9603.

Xiang, Z., Huguenard, J. R., & Prince, D. A. (1998). $GABA_A$ receptor mediated currents in interneurons and pyramidal cells of rat visual cortex. *J. Physiol., 506*, 715–730.

Received August 23, 2001; accepted March 22, 2002.